

Thesis Title

Institution Name

Author Name

Day Month Year

# Abstract

# Acknowledgements

# Notations

Abbreviations are given in small-caps. E.g sm instead of SM.

## CHAPTER 1

# Introduction

In particle physics we are concerned about small objects and their interactions. The smallest of these objects are referred to as *elemental particles*. Their dynamics are governed by the laws of nature. These laws are organised through symmetries, which are currently best described by the *Standard Model* (SM).

The SM classifies all known elementary particles and describes three of the four fundamental forces: the electromagnetic, weak and strong force. The particles representing matter are contained in two groups of fermionic, spin-1/2 particles. The former group, the leptons consist of: the electron ( $e$ ), the muon ( $\mu$ ), the tau ( $\tau$ ) and their corresponding neutrinos  $\nu_e$ ,  $\nu_\mu$  and  $\nu_\tau$ . The latter group, the quarks contain:  $u$ ,  $d$  (up and down, the so called light quarks),  $s$  (strange),  $c$  (charm),  $b$  (bottom or beauty) and  $t$  (top or truth). The three fundamental forces, the SM differentiates, are described through their carrier particles, the so-called bosons: the photon for the electromagnetic, the Z-or W-Boson for the weak and the gluon ( $g$ ) for the strong interaction. and strong ( $g$  gluon) interactions. The before mentioned Leptons solely interact through the electromagnetic and the weak force (also referred to as electroweak interaction), whereas the quarks additionally interact through the strong force. A short summary of the taxonomy of the SM can be seen in [fig. 1.1](#)

From a more mathematical point of view the SM is a gauge *Quantum Field Theory* (QFT). is the combination of *classical field theory*, *special relativity* and *quantum mechanics*. Its fundamental objects are ruled through its gauge-group  $SU(3) \times SU(2) \times U(1)$ . Each of its subgroups introduces a global and a local gauge symmetry. The global symmetry introduces the charges, which the

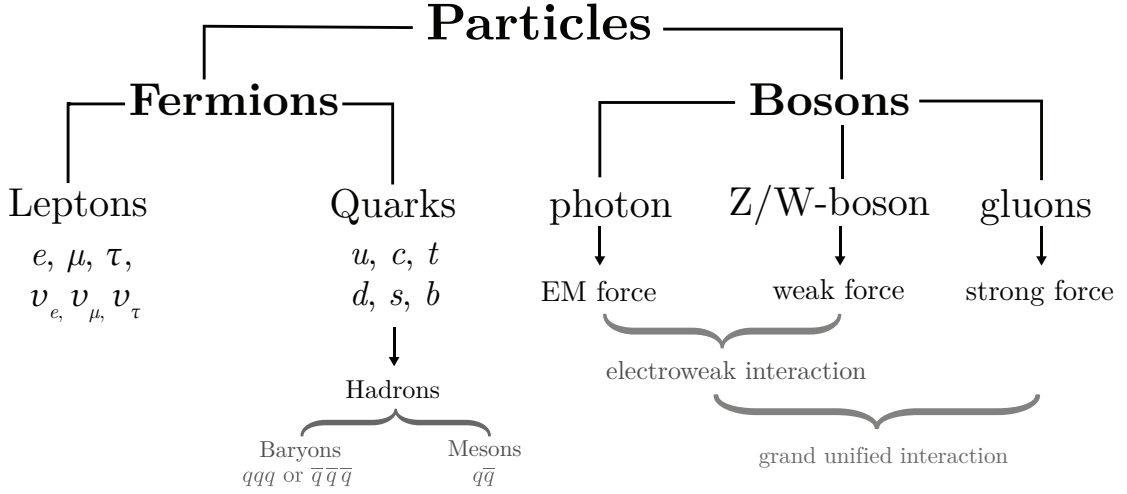


Figure 1.1: Taxonomy of the Standard Model.

fields are carrying. The local symmetry introduce the gauge-fields, which represent the previously mentioned force carriers. Naively every subgroup<sup>1</sup> of the gauge-group of the standard model is responsible for one of the three forces:

- U(1)** the *abelian* gauge group governs the representation of *quantum electrodynamics* (QED), which is commonly known as the electric force. Its global and local symmetry introduces the electric charge and the photon-field.
- SU(2)** Is the *non-abelian* symmetry group responsible for the weak-interaction. It introduces the  $W^+, W^-$  and Z bosons and the weak charge. The gauge groups U(1) and SU(2) have been combined to the *electroweak interaction*.
- SU(3)** The SU(3)-group is also *non-abelian* and governs the strong interactions, which are summarised in the theory of *Quantum Chromodynamics* (QCD). The group yields the three colour charges and due to its eight-dimensional adjoint-representation, eight different gluons.

Unfortunately we are still not able to include gravity, the last of the four forces, into the SM. There have been attempts to describe gravity through QFT with

<sup>1</sup>Actually U(1) and SU(2) have to be regarded as combined group to be mapped to the electromagnetic-and weak-force in form of the electroweak interaction.

the graviton, a spin-2 boson, as mediator, but there are unsolved problems with the renormalisation of general relativity (GR). Until now GR and quantum mechanics (QM) remain incompatible.

Apart from gravity no being included, the SM has a variety of flaws. One of them is being dependent on many parameters, which have to be measured accurately to perform high-precision physics. In total the Lagrangian of the SM contains 19 parameters. These parameters are represented by ten masses, four CKM-matrix parameters, the QCD-vacuum angle, the Higgs-vacuum expectation value and three gauge coupling constants. Highly accurate values with low errors are crucial for theoretical calculated predictions. One of the major error inputs of every theoretical output are uncertainties in these parameters. In this work we will focus on one of the parameters, namely the strong coupling  $\alpha_s$ .

The strong coupling is currently measured in six different ways: through  $\tau$ -decays, QCD-lattice computations, deep inelastic collider results and electroweak precision fits [45]. We have plotted the values of each of the methods in fig. 1.2. During this work we will focus on the subfield of  $\tau$ -decays to measure the value of the strong coupling  $\alpha_s(m_\tau)$  at the  $\tau$ -scale. We will see that in QCD the value of the coupling “constant” depends upon the scale. The  $\tau$  is an elementary particle with negative electric charge and a spin of  $1/2$ . Together with the lighter electron and muon it forms the group of charged Leptons<sup>2</sup>. Even though it is an elementary particle it decays via the weak interaction with a lifetime of  $\tau_\tau = 2.9 \times 10^{-13}$  s and has a mass of  $1776.86(12)$  MeV[45]. It is furthermore the only lepton massive enough to decay into hadrons, thus of interest for our QCD study. The final states of a decay are limited by conservation laws. In case of a  $\tau$ -decay they must conserve the electric charge ( $-1$ ) and invariant mass of the system. Thus, we can see from the corre-

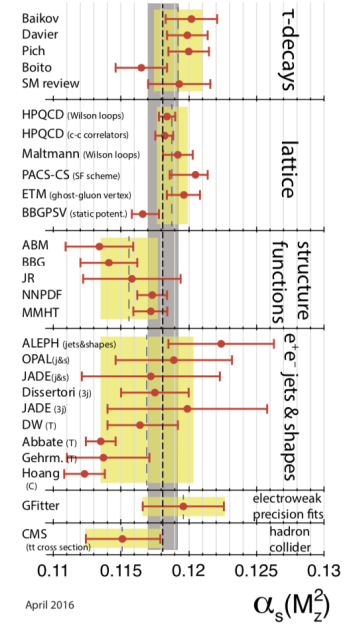


Figure 1.2: The six different subfields and their results for measuring the strong coupling  $\alpha_s$  [45].

<sup>2</sup>Leptons do not interact via the strong force.

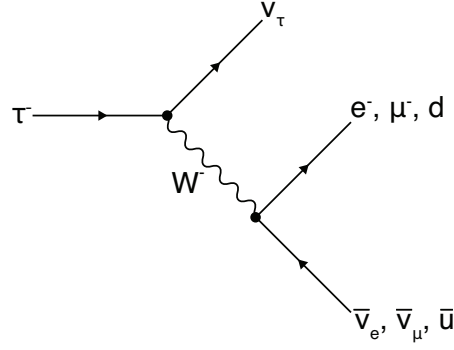


Figure 1.3: Feynman diagram of common decay of a  $\tau$ -lepton into pairs of lepton-antineutrino or quark-antiquark by the emission of a  $W$  boson.

Name	Symbol	Quark content	Rest mass (MeV)
Pion	$\pi^-$	$\bar{u}d$	139.570 61(24) MeV
Pion	$\pi^0$	$(u\bar{u} - d\bar{d})/\sqrt{2}$	134.9770(5) MeV
Kaon	$K^-$	$\bar{u}s$	493.677(16) MeV
Kaon	$K^0$	$d\bar{s}$	497.611(13) MeV
Eta	$\eta$	$(u\bar{u} + d\bar{d} - 2s\bar{s})/\sqrt{6}$	547.862(17) MeV

Table 1.1: List of mesons produced by a  $\tau$ -decay. Rare final states with branching Ratios smaller than 0.1 have been omitted. The list is taken from [17] with corresponding rest masses taken from [45].

sponding Feynman diagram [fig. 1.3](#)<sup>3</sup>, that the  $\tau$  decays by the emission of a  $W$ -boson and a tau-neutrino  $\nu_\tau$  into pairs of  $(e^-, \bar{\nu}_e)$ ,  $(\mu^-, \bar{\nu}_\mu)$  or  $(q, \bar{q})$ . We are foremost interested into the hadronic decay channels, meaning  $\tau$ -decays that have quarks in their final states. Quarks have never been measured isolated, but appear always in combination of *mesons* and *baryons*. Due to its mass of  $m_\tau \approx 1.8 \text{ GeV}$  the  $\tau$ -particle decays into light mesons (pions- $\pi$ , kaons- $K$ , and eta- $\eta$ , see [table 1.1](#)), which can be experimentally detected. The hadronic  $\tau$ -decay provides one of the most precise ways to determine the strong coupling [37] and is theoretically accessible to high precision within the framework of QCD.

<sup>3</sup>The  $\tau$ -particle can also decay into strange quarks or charm quarks, but these decays are rather uncommon due to the heavy masses of  $s$  and  $c$ .



The theory describing strong interactions is QCD. As the name suggest<sup>4</sup> QCD is characterised by the colour charge and is a non-abelian gauge theory with symmetry group  $SU(3)$ . Consequently every quark has next to its type one of the three colours blue, red or green and the colour force is mediated through eight gluons, which each being bi-coloured<sup>5</sup>, interact with quarks and each other. The strength of the strong force is given by the coupling constant  $\alpha_s$ , which depends on the renormalisation-scale  $\mu$ . We often chosen the renormalisation-scale in a way that the coupling constant  $\alpha_s(q)$  depends on the energy  $q^2$ . Thus the coupling varies with energy. It increases for low and decreases for high energies<sup>6</sup>. This behaviour has two main implications. The first one states, that for low energies the coupling is too strong for isolated quarks to exist. Until now we have not been able to observe an isolated quark and all experiments can only measure quark compositions. These bound states are called *hadrons* and consist of two or three quarks<sup>7</sup>, which are referred to as mesons<sup>8</sup> or baryons<sup>9</sup> respectively. This phenomenon, of quarks sticking together as hadrons is referred to as *confinement*. As the fundamental degrees of freedom of QCD are given by quarks and gluons, but the observed particles are hadrons we need to introduce the assumption of *quark-hadron duality* to match the theory to the experiment. This means that a physical quantity should be similarly describable in the hadronic picture or quark-gluon picture and that both descriptions are equivalent. As we will see in our work quark-hadron duality is violated for low energies. These so-called *duality violations* (DV) have an impact on our strong coupling determinations and can be dealt with either suppression or the inclusion of a model [12]. Throughout this work we will favour and argument for the former approach. The second implication concerns *Perturbative Theory* (PT). The lower the energies we deal with, the higher the value of the strong coupling and the contributions of *Non-Perturbative Theory* (NPT) effects. Currently there are three solutions to deal with *Non-Perturbative* (NP) effects:

- **Chiral Perturbation Theory** (CHPT): Introduced by Weinberg [48] in the

---

<sup>4</sup>Chromo is the Greek word for colour.

<sup>5</sup>Each gluon carries a colour and an anti-colour.

<sup>6</sup>In contrast to the electromagnetic force, where  $\alpha(q^2)$  decreases!

<sup>7</sup>There exist also so-called *Exotic hadrons*, which have more than three valence quarks.

<sup>8</sup>Composite of a quark and an anti-quark.

<sup>9</sup>Composite of three quarks or three anti-quarks.

late seventies. CHPT is an effective field theory constructed with a Lagrangian symmetric under a chiral-transformation in the limit of massless quarks. Its limitations are based in the chiral symmetry, which is only a good approximation for the light quarks  $u$ ,  $d$  and in some cases  $s$ .

- **Lattice QCD** (LQCD): Is the numerical approach to the strong force. Based on the Wilson Loops [49] we treat QCD on a finite lattice instead of working with continuous fields. LQCD has already many applications but is limited due to its computational expensive calculations.
- **QCD Sum Rules** (QCDSR): Was also introduced in the late seventies by Shifman, Vainshtein and Zakharov [43, 42]. It relates the observed hadronic picture to quark-gluon parameters through a dispersion relation and the use of the *Operator Product Expansion* (OPE), which treats NP effect through the definition of vacuum expectation values, the so-called *QCD condensates*. It is a precise method for extracting the strong coupling  $\alpha_s$  at low energies, although limited to the unknown higher order contributions of the OPE.

In this work we focus on the determination of the strong coupling  $\alpha_s$  within the framework of QCDSR for  $\tau$ -decays which has been exploited in the beginning of the nineties by Braaten, Narison and Pich [9]. Within this setup we can measure  $\alpha_s(m_\tau^2)$  at the  $m_\tau$  scale. As the strong coupling gets smaller at higher energies, so do the errors. Thus if we obtain the strong coupling at a low scale we will obtain high precision values at the scale of the Z-boson mass  $m_Z$ , which is the standard scale to compare  $\alpha_s$  values.

The QCDSR for the determination of  $\alpha_s$ , from low energies, contain three major issues.

1. There are two different approaches to treat perturbative and non-perturbative contributions. In particular, there is a significant difference between results obtained using fixed-order (FOPT) or contour improved perturbation theory (CIPT), such that analyses based on CIPT generally arrive at about 7% larger values of  $\alpha_s(m_{\tau^2})$  than those based on FOPT [45]. There have been a variety of analyses on the topic been performed [35, 11, 25] and we will favour the FOPT approach, but generously list our results for the CIPT framework.

2. There are several prescriptions to deal with the NP-contributions of higher order OPE condensates. Typically terms of higher dimension have been neglected, even if they knowingly contribute. In this work we will include every necessary OPE term.
3. Finally there are known DV leading to an ongoing discussion of the importance of contributions from DV. Currently there are two main approaches: Either we neglect them, arguing that they are sufficiently suppressed due to *pinched weights* [37] or model DV with sinusoidal exponentially suppressed function [12, 6, 8] introducing extra fitting parameters. We will argue for the former method, implementing pinched weights that sufficiently suppress DV contributions such as having only a negligible effect on our analysis.

In the first chapter of this work we want to summarise the necessary theoretical background for working with the QCDSR. Starting with the basics of QCD we want to motivate the *Renormalisation Group Equation* (RGE), which is responsible for the running of the strong coupling. We then continue with the some aspects of the two-point function and its usage in the dispersion relation, which connects the hadronic picture with the quark-gluon picture. . . .

## CHAPTER 2

# Theoretical Background

### 2.1 Quantum-chromodynamics

Since the formulation of QED in the end of the 40's it has been attempted to describe the strong nuclear force as a QFT, which has been achieved in the 70's as QCD [22, 21, 24, 38, 47]. QCD is a renormalisable QFT of the strong interaction, which fundamental fields are given by dirac spinors of spin-1/2, the so-called quarks, with a fractional electric charge of  $\pm 1/3$  or  $\pm 2/3$ . The theory furthermore contains gauge-fields of spin 1, which are chargeless, massless and referred to as gluons. The gluons are the force-mediators, which interact with quarks and themselves, in contrast to photons of QED, which interact only with fermions (see [fig. 2.1](#)).

The corresponding gauge-group of QCD is the non-abelian group SU(3). Each of the quark flavours u, d, c, s, t and b belongs to the fundamental representation of SU(3) and contains a triplet of fields  $\Psi$ .

$$\Psi = \begin{pmatrix} \Psi_1 \\ \Psi_2 \\ \Psi_3 \end{pmatrix} = \begin{pmatrix} \text{red} \\ \text{green} \\ \text{blue} \end{pmatrix} \quad (2.1.1)$$

The components of the triplet are the so-called colours<sup>1</sup> red, green and blue, which is referred to as *colour-charge*. The gluons belong to the adjoint representation of SU(3), contain an octet of fields and can be expressed using the

---

<sup>1</sup>The colour denomination is not gauge-invariant. After a colour gauge transformation the new colours are a linear combination of the old colours, which breaks gauge-symmetry.

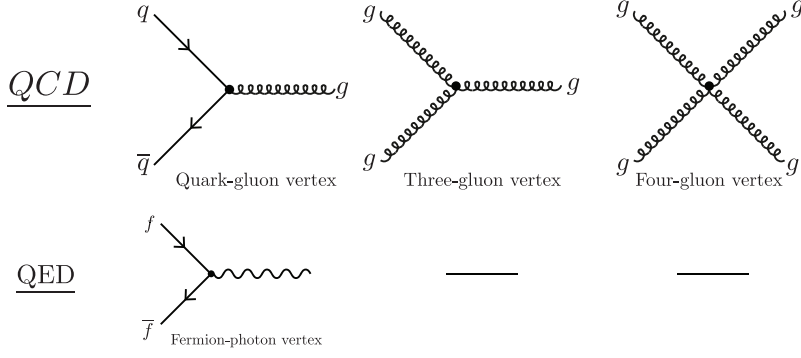


Figure 2.1: Feynman diagrams of the strong interactions with corresponding electromagnetic diagrams. We see that the gluons carry colour charge and thus couple to other gluons, which is not the case for the photons.

Flavour	Mass
u	3.48(24) MeV
d	6.80(29) MeV
s	130.0(18) MeV
c	1.523(18) GeV
b	6.936(57) GeV
t	173.0(40) GeV

Table 2.1: List of Quarks and their masses. The masses of the up, down, strange, charm and bottom quark are the renormalisation group invariant (RGI) quark masses and are quoted in the four-flavour theory ( $N_f = 2 + 1$ ) at the scale  $\mu = 2 \text{ GeV}$  in the  $\overline{\text{MS}}$  scheme and are taken from the *Flavour Lattice Averaging Group* [1]. The mass of the top quark is not discussed in [1] and has been taken from [45] from direct observations of top events.

Gell-Mann matrices  $\lambda_a$

$$B_\mu = B_\mu^a \lambda_a \quad a = 1, 2, \dots, 8 \quad (2.1.2)$$

The classical *Lagrange density* of QCD is given by [26, 33]:

$$\mathcal{L}_{\text{QCD}}(x) = -\frac{1}{4} G_{\mu\nu}^a(x) G^{\mu\nu a}(x) + \sum_A \left[ \frac{i}{2} \bar{q}^A(x) \gamma^\mu \overleftrightarrow{D}_\mu q^A(x) - m_A \bar{q}^A(x) q^A(x) \right], \quad (2.1.3)$$

with  $q^A(x)$  representing the quark fields and  $G_{\mu\nu}^a$  being the *gluon field strength tensor* given by:

$$G_{\mu\nu}^a(x) \equiv \partial_\mu B_\nu^a(x) - \partial_\nu B_\mu^a(x) + g f^{abc} B_\mu^b(x) B_\nu^c(x), \quad (2.1.4)$$

with  $f^{abc}$  as *structure constants* of the gauge-group  $\text{SU}(3)$  and  $\overleftrightarrow{D}_\mu$  as covariant derivative acting to the left and to the right. Furthermore we have

used  $A, B, \dots = 0, \dots, 5$  as flavour indices,  $a, b, \dots = 0, \dots, 8$  as colour indices and  $\mu, \nu, \dots = 0, \dots, 3$  as lorentz indices. Explicitly the Lagrangian writes:

$$\begin{aligned} \mathcal{L}_0(x) = & -\frac{1}{4} \left[ \partial_\mu G_\nu^a(x) - \partial_\nu G_\mu^a(x) \right] \left[ \partial^\mu G_a^\nu(x) - \partial^\nu G_a^\mu(x) \right] \\ & + \frac{i}{2} \bar{q}_\alpha^A(x) \gamma^\mu \partial_\mu q_\alpha^A(x) - \frac{i}{2} \left[ \partial_\mu \bar{q}_\alpha^A(x) \right] \gamma^\mu q_\alpha^A(x) - m_A \bar{q}_\alpha^A(x) q_\alpha^A(x) \\ & + \frac{g_s}{2} \bar{q}_\alpha^A(x) \lambda_{\alpha\beta}^a \gamma_\mu q_\beta^A(x) G_a^\mu(x) \\ & - \frac{g_s}{2} f_{abc} \left[ \partial_\mu G_\nu^a(x) - \partial_\nu G_\mu^a(x) \right] G_b^\mu(x) G_c^\nu(x) \\ & - \frac{g_s^2}{4} f_{abc} f_{ade} G_\mu^b(x) G_\nu^c(x) G_d^\mu(x) G_e^\nu(x) \end{aligned} \quad (2.1.5)$$

The first term is the kinetic term for the massless gluons. The next three terms are the kinetic terms for the quark field with different masses for each flavour. The rest of the terms are the interaction terms. The fifth term represents the interaction between quarks and gluons and the last two terms the self-interactions of gluon fields.

Having derived the Lagrangian leaves us with its quantisation. The dirac-spinors can be quantised as in QED without any problems. The  $\Psi(x)$  quantum field can be written as:

$$\Psi(x) = \int \frac{d^3p}{(2\pi)^3 2E(\vec{p})} \sum_\lambda \left[ u(\vec{p}, \lambda) a(\vec{p}, \lambda) e^{-ipx} + v(\vec{p}, \lambda) b^\dagger(\vec{p}, \lambda) e^{ipx} \right], \quad (2.1.6)$$

where the integration ranges over the positive sheet of the mass hyperboloid  $\Omega_+(m) = \{p | p^2 = m^2, p^0 > 0\}$ . The four spinors  $u(\vec{p}, \lambda)$  and  $v(\vec{p}, \lambda)$  are solutions to the dirac equations in momentum space

$$\begin{aligned} [\not{p} - m] u(\vec{p}, \lambda) &= 0 \\ [\not{p} + m] v(\vec{p}, \lambda) &= 0, \end{aligned} \quad (2.1.7)$$

with  $\lambda$  representing the helicity state of the spinors.

The quantisation of the gauge-fields are more cumbersome. One is forced to introduce supplementary non-physical fields, the so-called Faddeev-Popov ghosts  $c^a(x)$  [20].

The free propagators for the quark-, the gluon- and the ghost-fields are then

given by

$$\begin{aligned}
 iS_{\alpha\beta}^{(0)AB}(x-y) &\equiv \overline{q_\alpha^A(x)} q_\beta^B(y) \equiv \langle 0 | T \{ q_\alpha^A(x) \overline{q}_\beta^B(y) \} | 0 \rangle = \delta_{AB} \delta_{\alpha\beta} iS^{(0)}(x-y) \\
 iD_{ab}^{(0)\mu\nu}(x-y) &\equiv \overline{B_a^\mu(x)} B_b^\nu(y) \equiv \langle 0 | T \{ B_a^\mu(x) B_b^\nu(y) \} | 0 \rangle \equiv \delta_{ab} i \int \frac{d^4 k}{(2\pi)^4} D^{(0)\mu\nu}(k) e^{-ik(x-y)} \\
 &= i\delta_{ab} \int \frac{d^4 k}{(2\pi)^4} \frac{1}{k^2 + i\epsilon} \left[ -g_{\mu\nu} + (1-a) \frac{k_\mu k_\nu}{k^2 + i\epsilon} \right] e^{-ik(x-y)} \\
 i\tilde{D}_{ab}^{(0)}(x-y) &\equiv \overline{\phi_a(x)} \overline{\phi}_b(y) \equiv \langle 0 | T \{ \phi_a(x) \overline{\phi}_b(y) \} | 0 \rangle = \frac{i}{(2\pi)^4} \delta_{ab} \int d^4 q \frac{-1}{q^2 + i\epsilon} e^{-iq(x-y)} \\
 &\equiv \frac{i}{(2\pi)^4} \delta_{ab} \int d^4 q \tilde{D}^{(0)}(q) e^{-iq(x-y)},
 \end{aligned} \tag{2.1.8}$$

and the corresponding Feynman-rules have been displayed in [fig. 2.2](#).

### 2.1.1 Renormalisation Group

The perturbations of the QCD Lagrangian [2.1.3](#) lead to divergencies, which have to be *renormalised*. There are different approaches to ‘make’ these divergencies finite. The most popular one is **dimensional regularisation**.

In *dimensional regularisation* we expand the four space-time dimensions to arbitrary  $d$ -dimensions. Consequently the in QCD calculations appearing *Feynman integrals* have to be continued to  $D$ -dimensions like

$$\mu^{2\epsilon} \int \frac{d^D p}{(2\pi)^D} \frac{1}{[p^2 - m^2 + i0][(q-p)^2 - m^2 + i0]}, \tag{2.1.9}$$

where we introduced the scale parameter  $\mu$  to account for the extra dimensions.

*Physical quantities*<sup>2</sup> cannot depend on the renormalisation scale  $\mu$ . Therefore the derivative by  $\mu$  of a general physical quantity has to yield zero. The physical quantity  $R(q, a_s, m)$ , that depends on the external momentum  $q$ , the renormalised coupling  $a_s \equiv \alpha_s/\pi$  and the renormalised quark mass  $m$  can then be expressed as

$$\mu \frac{d}{d\mu} R(q, a_s, m) = \left[ \mu \frac{\partial}{\partial \mu} + \mu \frac{da_s}{da_s} \frac{\partial}{\partial a_s} + \mu \frac{dm}{dm} \frac{\partial}{\partial m} \right] R(q, a_s, m) = 0. \tag{2.1.10}$$

---

<sup>2</sup>Observables that can be measured.

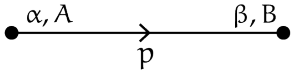
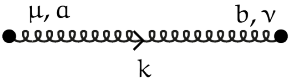
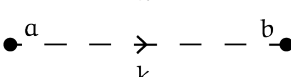
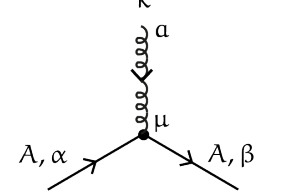
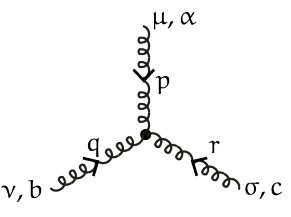
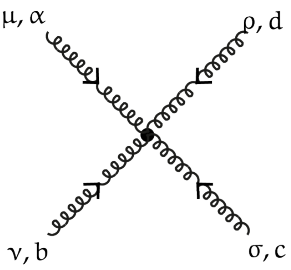
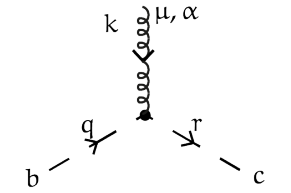
Quark propagator		$= \frac{i\delta_{\alpha\beta}\delta_{AB}}{\not{p} - m_A + i\epsilon}$
Gluon propagator		$= \frac{-i\delta_{ab}}{k^2 + i\epsilon} \left[ g^{\mu\nu} - (1 - a) \frac{k_\mu k_\nu}{k^2 + i\epsilon} \right]$
Ghost propagator		$= \frac{-\delta_{ab}}{k^2 + i\epsilon}$
Fermionic vertex		$= g \left( \frac{\lambda_a}{2} \right)_{\beta\alpha} \gamma^\mu$
Triple gluon vertex		$= -igf_{abc} [g_{\mu\nu}(p - q)_\sigma + g_{\nu\sigma}(q - r)_\mu + g_{\sigma\mu}(r - p)_\nu]$
Quartic gluon vertex		$= -g^2 [f_{abe}f_{cde}(g_{\mu\sigma}g_{\nu\rho} - g_{\mu\rho}g_{\nu\sigma}) + f_{ace}f_{bde}(g_{\mu\nu}g_{\sigma\rho} - g_{\mu\rho}g_{\nu\sigma}) + f_{ade}f_{cbe}(g_{\mu\sigma}g_{\nu\rho} - g_{\mu\nu}g_{\sigma\rho})]$
Ghost vertex		$= -igf_{abc}\tau^\mu$

Figure 2.2: QCD Feynman rules.



Equation 2.1.10 is referred to as **renormalisation group equation** and is the basis for defining the two *renormalisation group functions*:

$$\beta(a_s) \equiv -\mu \frac{d a_s}{d \mu} = \beta_1 a_s^2 + \beta_2 a_s^3 + \dots \quad \beta - \text{function} \quad (2.1.11)$$

$$\gamma(a_s) \equiv -\frac{\mu}{m} \frac{d m}{d \mu} = \gamma_1 a_s + \gamma_2 a_s^2 + \dots \quad \text{anomalous mass dimension.} \quad (2.1.12)$$

The coefficients of the  $\beta$ -function and the mass anomalous dimension are currently known up to the 5<sup>th</sup> order and listed in the appendix 6.1.

### Running gauge coupling

The  $\beta$ -function and the anomalous mass dimension are responsible for the running of the strong coupling and the running of the quark mass respectively. In this section we will shortly review the  $\beta$ -function and its implications on the strong coupling, whereas in the following section we will discuss the anomalous-mass dimension.

Regarding the  $\beta$ -function we notice, that  $a_s(\mu)$  is not a constant, but *runs* by varying its scale  $\mu$ . Lets observe the running of the strong coupling constant by integrating the  $\beta$ -function

$$\int_{a_s(\mu_1)}^{a_s(\mu_2)} \frac{d a_s}{\beta(a_s)} = - \int_{\mu_1}^{\mu_2} \frac{d \mu}{\mu} = \log \frac{\mu_1}{\mu_2}. \quad (2.1.13)$$

To analytically evaluate the above integral we can approximate the  $\beta$ -function to first order, with the known coefficient

$$\beta_1 = \frac{1}{6}(11N_c - 2N_f), \quad (2.1.14)$$

yielding

$$a_s(\mu_2) = \frac{a_s(\mu_1)}{\left(1 - a_s(\mu_1)\beta_1 \log \frac{\mu_1}{\mu_2}\right)}. \quad (2.1.15)$$

As we have three colours ( $N_c = 3$ ) and six flavours ( $N_f = 6$ ) the first  $\beta$ -function 2.1.11 is positive. Thus for  $\mu_2 > \mu_1$   $a_s(\mu_2)$  decreases logarithmically and vanishes for  $\mu_2 \rightarrow \infty$ . This behaviour is known as *asymptotic freedom* and leads to *confinement*.

Asymptotic freedom states, that for high energies (small distances), the strong coupling becomes diminishing small and quarks and gluons do not interact.

Thus in isolated baryons and mesons the quarks are separated by small distances, move freely and do not interact. On the other hand we are not able to separate the quarks in a meson or baryon. No quark has been detected as single particle yet. This is qualitatively explained with the gluon field carrying colour charge. These gluons form so-called *flux-tubes* between quarks, which cause a constant strong force between particles regardless of their separation. Consequently the energy needed to separate quarks is proportional to the distance between them and at some point there is enough energy to favour the creation of a new quark pair. Thus before separating two quarks we create a quark-antiquark pair. As a result we will probably never be able to observe an isolated quark. This phenomenon is referred to as colour confinement or simply confinement.

### Running quark mass

Not only the coupling but also the masses carry an energy dependencies, which is governed by the *anomalous mass dimension*  $\gamma(a_s)$ .

The properties of the running quark mass can be derived similar to the gauge coupling. Starting from integrating the *anomalous mass dimension* [eq. 2.1.12](#)

$$\log \frac{m(\mu_2)}{m(\mu_1)} = \int_{a_s(\mu_1)}^{a_s(\mu_2)} da_s \frac{\gamma(a_s)}{\beta(a_s)} \quad (2.1.16)$$

we can approximate the *anomalous mass dimension* to first order and solve the integral analytically [\[41\]](#)

$$m(\mu_2) = m(\mu_1) \left( \frac{a(\mu_2)}{a(\mu_1)} \right)^{\frac{\gamma_1}{\beta_1}} (1 + \mathcal{O}(\beta_2, \gamma_2)). \quad (2.1.17)$$

As  $\beta_1$  and  $\gamma_1$  (see [6.2](#)) are positive the quark mass decreases with increasing  $\mu$ . The general relation between different scales is given by

$$m(\mu_2) = m(\mu_1) \exp \left( \int_{a_s(\mu_1)}^{a_s(\mu_2)} da_s \frac{\gamma(a_s)}{\beta(a_s)} \right) \quad (2.1.18)$$

and can be solved numerically to run the quark mass to the needed scale  $\mu_2$ .

QCD in general has a precision problem caused by uncertainties and largeness of the strong coupling constant  $\alpha_s$ . The fine-structure constant (the coupling QED) is known to eleven digits, whereas the strong coupling is only known

to about four. Furthermore for low energies the strong coupling constant is much larger than the fine-structure constant. E.g. at the Z-mass, the standard mass to compare the strong coupling, we have an  $\alpha_s$  of 0.11, whereas the fine structure constant would be around 0.007. Consequently to use PT we have to calculate our results to much higher orders, including tens of thousands of Feynman diagrams, in QCD to achieve a precision equal to QED. For even lower energies, around 1 GeV, the strong coupling reaches a critical value of  $\approx 0.5$  leading to a break down of PT.

In this work we try to achieve a higher precision in the value of  $\alpha_s$ . Our method to measure the strong coupling are the QCDSR, which in our case make use of the *two-point function* for which we will devote the following section

### 2.1.2 Two-Point function

The vacuum expectation value of the product of the conserved Noether current  $J_\mu(x)$  at different space-time points  $x$  and  $y$  is known as the **two-point function** (or simply **correlator**)

$$\Pi_{\mu\nu}(q^2) = \int d^4x e^{iqx} \langle 0 | J_\mu(x) J_\nu(0) | 0 \rangle, \quad (2.1.19)$$

where the Noether current is given by

$$J_\mu(x) = \bar{q}(x) \Gamma q(x), \quad (2.1.20)$$

where  $\Gamma$  can be any of the following dirac matrices  $\Gamma \in \{1, i\gamma_5, \gamma_\mu, \gamma_\mu\gamma_5\}$ , specifying the quantum number of the current (S: *scalar*, P: *pseudo-Scalar*, V: *vectorial*, A: *axial-vectorial*, respectively).

The vector correlator  $\Pi_{\mu\nu}(q^2)$  can be Lorentz decomposed to a scalar function  $\Pi(q^2)$ . There are only two possible terms that can reproduce the second order tensor  $q_\mu q_\nu$  and  $q^2 g_{\mu\nu}$ . The sum of both multiplied with two arbitrary functions  $A(q^2)$  and  $B(q^2)$  yields

$$\Pi_{\mu\nu}(q^2) = q_\mu q_\nu A(q^2) + q^2 g_{\mu\nu} B(q^2). \quad (2.1.21)$$

By making use of the *Ward-identity*

$$\begin{aligned}
 q^\mu \Pi_{\mu\nu} &= \int d^4x q^\mu e^{iq \cdot x} \langle 0 | J_\mu(x) J_\nu(0) | 0 \rangle \\
 &= -i \int d^4x i q^\mu e^{iq \cdot x_\nu} \langle 0 | J_\mu(x) J_\nu(0) | 0 \rangle \\
 &= i \int d^4x e^{iq \cdot x} \langle 0 | \partial_\mu (J_\mu(x)) J_\nu(0) | 0 \rangle \\
 &= 0, \quad \text{with} \quad \partial_\mu J_\mu(x) = 0,
 \end{aligned} \tag{2.1.22}$$

where we used  $i q^\mu e^{iq \cdot x_\nu} = \partial_\mu e^{iq \cdot x_\nu}$  in the second and integration by parts in the third line. The Ward identity is dependent on the conserved Noether-current  $J_\mu$  and thus only holds for same flavour quarks. With the Ward-identity we are able to demonstrate, that the two arbitrary functions are related

$$\begin{aligned}
 q^\mu q^\nu \Pi_{\mu\nu} &= q^4 A(q^2) + q^4 B(q^2) = 0 \\
 \implies A(q^2) &= -B(q^2).
 \end{aligned} \tag{2.1.23}$$

Thus redefining  $A(q^2) \equiv \Pi(q^2)$  we expressed the correlator as a scalar function

$$\Pi_{\mu\nu}(q^2) = (q_\mu q_\nu - q^2 g_{\mu\nu}) \Pi(q^2). \tag{2.1.24}$$

The scalar QCD two point function can then be described by the spectrum of hadronic states. The correlator is then related to an integral over the *spectral function*  $\rho(s)$  via the *Källén-Lehmann spectral representation* [28, 32], which is known since the early fifties

$$\Pi(q^2) = \int_0^\infty ds \frac{\rho(s)}{s - q^2 - i\epsilon}. \tag{2.1.25}$$

Equation 2.1.25 is referred to as *dispersion relation* analogous to similar relations which arise for example in electrodynamics and defines the *spectral function* (a derivation can be found in [39])

$$\rho(s) = \frac{1}{\pi} \text{Im} \Pi(s). \tag{2.1.26}$$

Until now we connected theoretical correlator with the measurable hadronic spectrum. Nevertheless the analytic properties of the correlators have to be discussed as the function has discontinuities.

The main contribution from the spectral function given in eq. 2.1.25 are the hadronic final states

$$2\pi\rho(m^2) = \sum_n \langle 0 | J_\mu(x) | n \rangle \langle n | J_\nu(y) \rangle (2\pi^2)^4 \delta^{(4)}(p - p_n), \tag{2.1.27}$$

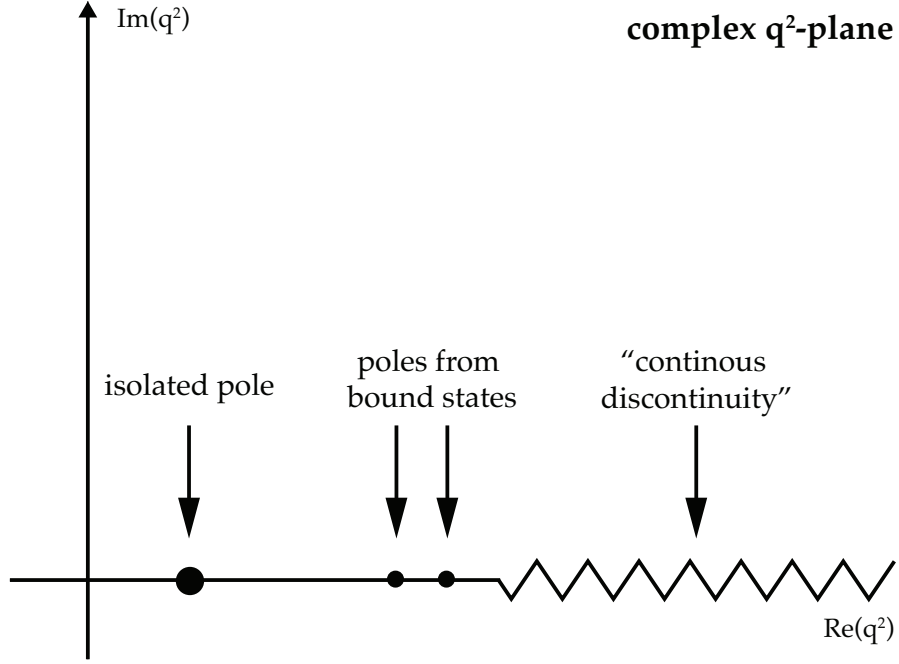


Figure 2.3: Analytic structure in the complex  $q^2$ -plane of the Fourier transform of the two-point function. The hadronic final states are responsible for poles appearing on the real-axis. The one-particle states contribute as isolated pole and the multi-particle states contribute as bound-states poles or a continuous “discontinuity cut” [34].

which lead to a series of continuous poles on the positive real axis for the two-point function (see Fig. 2.3). These discontinuities can be tackled with *Cauchy’s theorem*, which we will apply in section 2.1.4.

Having dealt exclusively with the perturbative part of the theory, we have to discuss non-perturbative contributions, as QCD is known to have non-negligible contributions. Thus before continuing with the *Sum Rules* we need a final ingredient the *Operator Product Expansion* (OPE), which treats the non-perturbative contributions of our theory.

### 2.1.3 Operator Product Expansion

The OPE was introduced by Wilson in 1969 [50]. The expansion states that non-local operators can be rewritten into a sum of composite local operators and

their corresponding coefficients:

$$\lim_{x \rightarrow y} \mathcal{O}_1(x) \mathcal{O}_2(y) = \sum_n C_n(x-y) \mathcal{O}_n(x), \quad (2.1.28)$$

where  $C_n(x-y)$  are the so-called *Wilson-coefficients*.

The OPE lets us separate short-distance from long-distance effects. In PT we can only amount for short-distances, which are equal to height energies, where the strong-coupling  $\alpha_s$  is small. Consequently the OPE decodes the long-distance effects in the higher dimensional operators.

The form of the composite operators are dictated by Gauge- and Lorentz symmetry. Thus we can only make use of operators of even dimension. The operators up to dimension six are given by [33]

$$\begin{aligned} \text{Dimension 0: } & \mathbb{1} \\ \text{Dimension 4: } & : m_i \bar{q} q : \\ & : G_a^{\mu\nu}(x) G_{\mu\nu}^a(x) : \\ \text{Dimension 6: } & : \bar{q} \Gamma q \bar{q} \Gamma q : \\ & : \bar{q} \Gamma \frac{\lambda^a}{2} q_\beta(x) \bar{q} \Gamma \frac{\lambda^a}{2} q : \\ & : m_i \bar{q} \frac{\lambda^a}{2} \sigma_{\mu\nu} q G_a^{\mu\nu} : \\ & : f_{abc} G_a^{\mu\nu} G_b^{\nu\delta} G_c^{\delta\mu} :, \end{aligned} \quad (2.1.29)$$

where  $\Gamma$  stands for one of possible dirac matrices (as seen eq. 2.1.20). As all the operators appear normal ordered they vanish by definition in PT. Consequently they appear as *condensates* in NPT QCD like quark-condensate  $\langle \bar{q} q \rangle$  or the gluon-condensate  $\langle a G G \rangle$  (both of dimension four). These non-vanishing condensates characterise the QCD-vacuum.

As we work with dimensionless functions (e.g. the correlator  $\Pi$ ) in Sum Rules, the r.h.s. of eq. 2.1.28 has to be dimensionless. Consequently the Wilson-coefficients have to cancel the dimension of the operator with their inverse mass dimension. To account for the dimensions we can make the inverse momenta explicit

$$\Pi_{V/A}^{\text{OPE}}(s) = \sum_{D=0,2,4,\dots} \frac{c^{(D)} \langle \mathcal{O}^{(D)}(x) \rangle}{-s^{D/2}}, \quad (2.1.30)$$

where we used  $C^{(D)} = c/(-s)^{D/2}$  with  $D$  being the dimension. Consequently the OPE should converge with increasing dimension for sufficiently large momenta  $s$ .

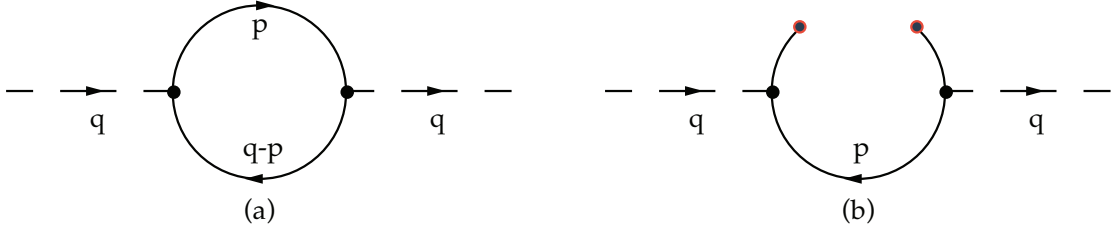


Figure 2.4: Feynman diagrams of the perturbative (a) and the quark-condensate (b) contribution. The upper part of the right diagram is not wick-contracted and responsible for the condensate.

Let's show how the OPE contributions are calculated with a the “standard example” (following [33]), where we compute the perturbative and quark-condensate Wilson-coefficients for the  $\rho$ -meson. For the  $\rho$ -meson, which is composed of  $u$  and  $d$  quarks, the current of eq. 2.1.19 takes the following form

$$j^\mu(x) = \frac{1}{2} \left( [\bar{u} \gamma^\mu u](x) - \bar{d} \gamma^\mu d](x) \right). \quad (2.1.31)$$

In fig. 2.4 we draw the Feynman-diagram, from which we can take the uncontracted mathematical expression for the scalar correlator

$$\begin{aligned} \Pi(q^2) = & -\frac{i}{4q^2(D-1)} \int d^D x e^{iqx} \langle \Omega | T \{ : \bar{u}(x) \gamma^\mu u(x) - \bar{d}(x) \gamma^\mu d(x) : \\ & \times : \bar{u}(0) \gamma_\mu u(0) - \bar{d}(0) \gamma_\mu d(0) : \} \rangle. \end{aligned} \quad (2.1.32)$$

Using Wick's theorem we can contract all of the fields and calculate the first term of the OPE (1), which represents the perturbative contribution of the OPE (1)

$$\begin{aligned} \Pi(q^2) = & \frac{i}{4q^2(D-1)} (\gamma^\mu)_{ij} (\gamma_\mu)_{kl} \int d^D x e^{iqx} \\ & \times \left[ \overline{u_{j\alpha}(x) \bar{u}_{k\beta}(0)} \cdot \overline{u_{l\beta}(0) \bar{u}_{i\alpha}(x)} + (u \rightarrow d) \right] \\ & = \frac{3}{8\pi^2} \left[ \frac{5}{3} - \log \left( -\frac{q^2}{\nu^2} \right) \right]. \end{aligned} \quad (2.1.33)$$

To calculate the higher dimensional contributions of the OPE we use the same techniques as before, but leave some of the fields uncontracted. For the quark-condensate, which we want to derive for tree-level, we leave two fields uncon-

tracted

$$\begin{aligned} \Pi(q^2) = & \frac{i}{4q^2(D-1)} (\gamma^\mu)_{ij} (\gamma_\mu)_{kl} \int d^D x e^{iqx} \left[ \right. \\ & + \overbrace{u_{j\alpha}(x) \bar{u}_{k\beta}(0)} \cdot \langle \Omega | : \bar{u}_{i\alpha}(x) u_{l\beta}(0) : | \Omega \rangle \\ & \left. + \overbrace{u_{l\beta}(0) \bar{u}_{i\alpha}(x)} \cdot \langle \Omega | : \bar{u}_{k\beta}(0) u_{j\alpha}(x) : | \Omega \rangle + (u \rightarrow d) \right]. \end{aligned} \quad (2.1.34)$$

The non contracted fields can then be expanded in  $x$

$$\begin{aligned} \langle \Omega | : \bar{q}(x) q(0) : | \Omega \rangle = & \langle \Omega | : \bar{q}(0) q(0) : | \Omega \rangle \\ & + \langle \Omega | : [\partial_\mu \bar{q}(0)] q(0) : | \Omega \rangle x^\mu + \dots \end{aligned} \quad (2.1.35)$$

and redefined to a more elegant notation

$$\langle \bar{q} q \rangle \equiv \langle \Omega | : \bar{q}(0) q(0) : | \Omega \rangle. \quad (2.1.36)$$

The finally result can be expressed as

$$\Pi_{(\rho)}(q^2) = \frac{1}{2} \frac{1}{(-q^2)^2} \left[ m_u \langle \bar{u} u \rangle + m_d \langle \bar{d} d \rangle \right]. \quad (2.1.37)$$

The usage of the OPE and its validity is far from obvious. We are deriving the OPE from matching the Wilson-coefficients to Feynman-graph analyses. These Feynman-graphs are calculated perturbatively but the coefficients with dimension  $D > 0$  correspond to NPT condensates!

Having gathered all of the necessary concepts we can close the gap between the theory and experiment in the last section of the introduction: QCDSR.

#### 2.1.4 Sum Rules

To relate the measurable hadronic final states of a QCD process (e.g.  $\tau$ -decays into hadrons) to a theoretical calculable QCDSR have been employed by Shifman in the late seventies [43].

The sum rules are a combination of the two-point function, its analyticity, the OPE, a dispersion relation, the optical theorem and quark hadron duality.

The previously introduced two-point function [eq. 2.1.19](#) is generally described by the OPE to account for NPT effects.

$$\Pi(q^2) = \Pi^{\text{OPE}}(q^2). \quad (2.1.38)$$



Furthermore it is related to the theoretical spectral function  $\rho(s)$  via a dispersion relation (eq. 2.1.25). Using QCD we are computing interactions based on quarks and gluons, but as we have seen (confinement), we are only able to observe hadrons. Consequently to connect the theory to the experiment we have to assume **quark-hadron duality**<sup>3</sup>, which implies that physical quantities can be described equally good in the hadronic or in the quark-gluon picture. Thus we rewrite the dispersion relation eq. 2.1.25 as

$$\Pi_{\text{th}}^{\text{OPE}}(q^2) = \int_0^\infty \frac{\rho_{\text{exp}}(q^2)}{(s - q^2 - i\epsilon)}, \quad (2.1.39)$$

where we connected the theoretical correlator  $\Pi_{\text{th}}$  with the experimental measurable spectral function  $\rho_{\text{exp}}$ .

We have seen, that the theoretical description of the correlator  $\Pi_{\text{th}}$  contains poles on the real axis. Unfortunately the experimental data  $\rho_{\text{exp}}$  is solely accessible on the positive real axis. As a result we have to make use of Cauchy's theorem to access the theoretical values of the two-point function close to the positive real axis (see section 2.1.4), which is given by

$$\int_{\mathcal{C}} f(z) dz = 0, \quad (2.1.40)$$

where  $f(z)$  is an analytic function on a closed contour  $\mathcal{C}$ .

The final ingredient of the QCD sum rules is the *optical theorem*, relating experimental data with the imaginary part of the correlator (the spectral function  $\rho(s)$ ).

In total, with the help Cauchy's theorem, the QCD sum rules can be summed up in the following expression

$$\frac{1}{\pi} \int_0^\infty \frac{\rho_{\text{exp}}(t)}{t - s} dt = \frac{1}{\pi} \oint_{\mathcal{C}} \frac{\text{Im } \Pi_{\text{OPE}}(t)}{t - s} dt, \quad (2.1.41)$$

where the l.h.s. is given by the experiment and the r.h.s. can be theoretically evaluated by applying the OPE of the correlator  $\Pi_{\text{OPE}}(s)$ .

---

<sup>3</sup>Or simply duality.

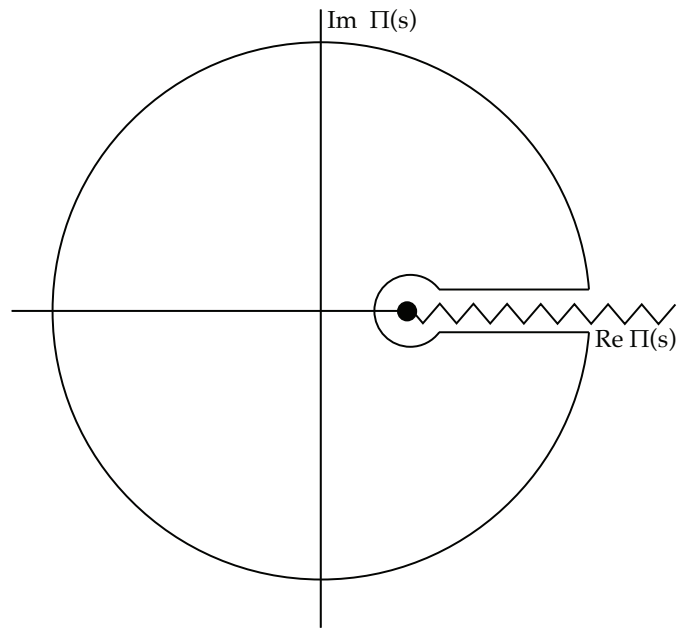


Figure 2.5: Analytical structure of  $\Pi(s)$  with the used contour  $\mathcal{C}$  for the final QCD Sum Rule expression [eq. 2.1.41](#).

## CHAPTER 3

# $\tau$ -decay into hadrons

In this chapter we prepare our QCD analysis of  $\tau$ -decays from which we will extract a value for the strong coupling constant  $\alpha_s$  at the  $m_\tau$ -scale. The central phenomenon to this analysis are the  $\tau$ -decays into hadrons. We will build on the previously presented QCDSR (eq. 2.1.41):

$$\frac{1}{\pi} \int_0^\infty \frac{\rho_{\text{exp}}(t)}{t-s} dt = \frac{1}{\pi} \oint_{\mathcal{C}} \frac{\text{Im} \Pi_{\text{OPE}}(t)}{t-s} dt. \quad (3.0.1)$$

Here we need to connect the experimental data  $\rho_{\text{exp}}$  given by the ALEPH-group with the theoretical accessible, imaginary part of the two-point function  $\Pi_{\text{OPE}}$ . Starting with the central phenomenon to extract the strong coupling at low energies,  $\tau$ -decays into hadrons we will express the correlator in terms of the OPE. Within this process we will talk about problems and solutions concerning PT and DV.

### 3.1 $\tau$ -decays into hadrons

The  $\tau$ -lepton is the only lepton heavy enough to decay into Hadrons. It permits one of the most precise determinations of the strong coupling  $\alpha_s$ . The inclusive  $\tau$ -decay ratio

$$R_\tau = \frac{\Gamma(\tau \rightarrow \nu_\tau + \text{Hadrons})}{\Gamma(\tau \rightarrow \nu_\tau e^+ e^-)} \quad (3.1.1)$$

can be precisely calculated and is sensitive to  $\alpha_s$ . Due to low the mass of the  $\tau$ -lepton  $m_\tau \approx 1.8 \text{ GeV}$   $\tau$ -decays are excellent for performing a low-energy QCD analysis. The theoretical expression of the hadronic  $\tau$ -decay ratio was first derived by [46], using current algebra, a more recent derivation making

use of the *optical theorem* can be taken from [41]. The inclusive ratio is then given by:

$$R_\tau(s) = 12\pi \int_0^{m_\tau} \frac{ds}{m_\tau^2} \left(1 - \frac{s}{m_\tau^2}\right) \left[ \left(1 + 2\frac{s}{m_\tau^2}\right) \text{Im} \Pi^{(T)}(s) + \text{Im} \Pi^{(L)}(s) \right], \quad (3.1.2)$$

where  $\text{Im} \Pi$  is the two-point function (see section 2.1.2). In the case of  $\tau$ -decays we only have to consider vector (V) and axial-vector contributions (A) of decays into up, down and strange quarks. Thus taking  $i, j$  as the flavour indices for the light quarks (u, d and s) we can express the correlator as

$$\Pi_{\mu\nu,ij}^{V/A}(s) \equiv i \int d^4x e^{ipx} \langle \Omega | T \{ J_{\mu,ij}^{V/A}(x) J_{\nu,ij}^{V/A}(0)^\dagger \} | \Omega \rangle, \quad (3.1.3)$$

with  $|\Omega\rangle$  being the physical vacuum. The vector and axial-vector currents are then distinguished by the corresponding dirac-matrices ( $\gamma_\mu$  and  $\gamma_\mu \gamma_5$ ) given by

$$J_{\mu,ij}^V(x) = \bar{q}_j(x) \gamma_\mu q_i(x) \quad \text{and} \quad J_{\mu,ij}^A(x) = \bar{q}_j(x) \gamma_\mu \gamma_5 q_i(x). \quad (3.1.4)$$

The two-point function can be decomposed into its vector and axial-vector contributions, but also into transversal and longitudinal components. We will give now both of these decompositions and relate them, which has some implications for a common used approximation: the **chiral limit**, where the quark masses are taken to 0 ( $m_q \rightarrow 0$ ).

Starting with the decomposition into vector, axial-vector, scalar (S) and pseudo-scalar (P) components we can write [10, 27]

$$\begin{aligned} \Pi^{\mu\nu}(q^2) &= (q^\mu q^\nu - q^2 g^{\mu\nu}) \Pi^{V,A}(q^2) + \frac{g^{\mu\nu}}{q^2} (m_i \mp m_j) \Pi^{S,P}(q^2) \\ &\quad + g^{\mu\nu} \frac{(m_i \mp m_j)}{q^2} [\langle \bar{q}_i q_i \rangle \mp \langle \bar{q}_j q_j \rangle], \end{aligned} \quad (3.1.5)$$

which is composed of a vector  $\Pi^{V,A}$  and scalar  $\Pi^{S,P}$  part. The third term are corrections arising due to the physical vacuum  $|\Omega\rangle$ . The latter decomposition rewrites the correlator  $\Pi^{\mu\nu}(q^2)$  into transversal and longitudinal components:

$$\Pi^{\mu\nu}(q^2) = (q^\mu q^\nu - g^{\mu\nu} q^2) \Pi^{(T)}(q^2) + q^\mu q^\nu \Pi^{(L)}(q^2). \quad (3.1.6)$$

With the two decompositions eq. 3.1.5 and eq. 3.1.6 we can now identify the longitudinal components of the correlator as being purely scalar, by multiplying eq. 3.1.5 by two four-momenta and making use of the Ward-identity eq. 2.1.22 we can write

$$q_\mu q_\nu \Pi^{\mu\nu}(q^2) = (m_i \mp m_j)^2 \Pi^{S,P}(q^2) + (m_i \mp m_j) [\langle \bar{q}_i q_i \rangle \mp \langle \bar{q}_j q_j \rangle], \quad (3.1.7)$$

which then can be related to the longitudinal component of [eq. 3.1.6](#) by comparison of the two equations

$$q_\mu q_\nu \Pi^{\mu\nu}(q^2) = q^4 \Pi^{(L)}(q^2) = s^2 \Pi^{(L)}(s) \quad \text{with} \quad s \equiv q^2. \quad (3.1.8)$$

In a more eloquent way this can be expressed as

$$s^2 \Pi^{(L)}(s) = (m_i \mp m_j)^2 \Pi^{(S,P)}(s) + (m_i \mp m_j) [\langle \bar{q}_i q_i \rangle \mp \langle \bar{q}_j q_j \rangle], \quad (3.1.9)$$

where we can see, that all mass terms are related to the longitudinal component of the correlator. By defining a combination of the transversal and longitudinal correlator

$$\Pi^{(T+L)}(s) \equiv \Pi^{(T)}(s) + \Pi^{(L)}(s) \quad (3.1.10)$$

we can additionally relate the transversal and vectorial components via

$$\Pi^{\mu\nu}(s) = \underbrace{(q^\mu q^\nu - g^{\mu\nu} q^2) \Pi^{(T)}(s) + (q^\mu q^\nu - g^{\mu\nu} q^2) \Pi^{(L)}(s)}_{=(q^\mu q^\nu - g^{\mu\nu} q^2) \Pi^{(T+L)}(s)} + \frac{g^{\mu\nu} s^2}{q^2} \Pi^{(L)}(s), \quad (3.1.11)$$

such that

$$\Pi^{(V,A)}(s) = \Pi^{(T)}(s) + \Pi^{(L)}(s) = \Pi^{(T+L)}, \quad (3.1.12)$$

where the vector/ axial-vector component of the correlator is now related to the newly defined transversal and longitudinal combination of the correlator. As the  $\tau$ -decays, with the limiting factor of the  $\tau$ -mass, can only decay into light quarks we will often neglect the quark masses and work in the so called chiral limit. In the chiral limit the longitudinal component, which is proportional to the quark masses, of the correlator vanishes.

Examining the inclusive ratio  $R_\tau$  in [eq. 3.1.1](#), we note that we have to deal with a problematic integral over the real axis of  $\Pi(s)$  from 0 up to  $m_\tau$ . The integral is problematic for two reasons:

- **Perturbative Quantum Chromodynamics** (pQCD) and the OPE breaks down for low energies (over which we have to integrate).
- The positive Euclidean axis of  $\Pi(s)$  has a discontinuity cut and can theoretically not be evaluated (see [section 2.1.2](#)).

To literally circumvent the former issue we make use of *Cauchy's Theorem* [eq. 2.1.40](#). For the latter we will apply so-called *pinched weights*.

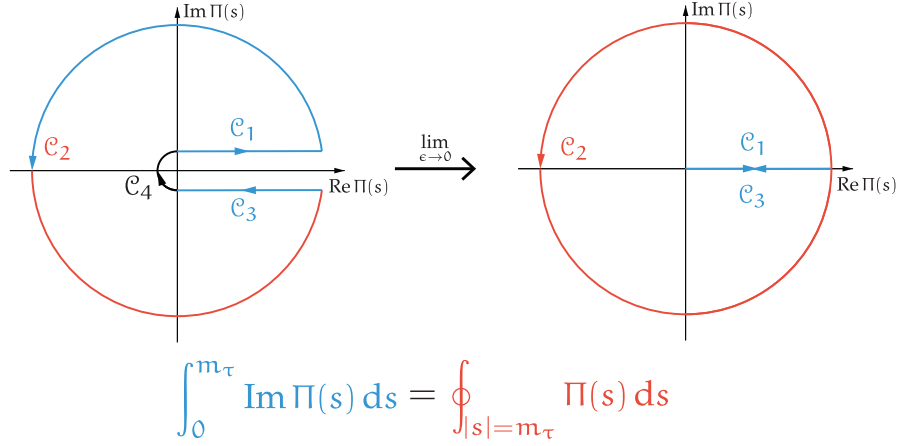


Figure 3.1: Visualization of the usage of Cauchy's theorem to transform eq. 3.1.2 into a closed contour integral over a circle of radius  $m_\tau^2$ .

### 3.2 Rescuing pQCD with Cauchy's theorem

We will make use of Cauchy's theorem to rewrite the definite integral of eq. 3.1.2 into a contour integral over a closed circle with radius  $m_\tau^2$ . The closed contour consists of four line integrals, which have been visualized in fig. 3.1. Summing over the four line integrals, performing a *analytic continuation* of the two-point correlator  $\Pi(s) \rightarrow \Pi(s + i\epsilon)$  and finally taking the limit of  $\epsilon \rightarrow 0$  gives us the needed relation between eq. 3.1.2 and the closed contour:

$$\begin{aligned}
 \oint_{s=m_\tau} \Pi(s) &= \int_0^{m_\tau} \Pi(s + i\epsilon) + \int_{C_2} \Pi(s) ds + \int_{m_\tau}^0 \Pi(s - i\epsilon) ds + \int_{C_4} \Pi(s) ds \\
 &= \int_0^{m_\tau} \Pi(s + i\epsilon) - \Pi(s - i\epsilon) ds + \int_{C_2} \Pi(s) ds + \int_{C_4} \Pi(s) ds \\
 &= \int_0^{m_\tau} \Pi(s + i\epsilon) - \overline{\Pi(s + i\epsilon)} + \int_{C_2} \Pi(s) ds + \int_{C_4} \Pi(s) ds \\
 &\stackrel{\lim_{\epsilon \rightarrow 0}}{=} 2i \int_0^{m_\tau} \text{Im } \Pi(s) ds + \oint_{s=m_\tau} \Pi(s) ds
 \end{aligned} \tag{3.2.1}$$

where we made use of  $\Pi(z) = \overline{\Pi(\bar{z})}$  (due to  $\Pi(s)$  is analytic) and  $\Pi(z) - \overline{\Pi(\bar{z})} = 2i \text{Im } \Pi(z)$ . The result can be rewritten in a more intuitive form, which we also visualized in fig. 3.1

$$\int_0^{m_\tau} \Pi(s) ds = \frac{i}{2} \oint_{s=m_\tau} \Pi(s) ds \tag{3.2.2}$$

Due to the circle-contour we can avoid low energies at which pQCD would break down.

To deal with the latter issue we have to suppress the contributions of the correlator close to the positive real axis, which can be achieved by introducing weight functions, which suppress contributions of the two-point function close to the positive real axis.

Finally combining eq. 3.2.2 with eq. 3.1.2 we get

$$R_\tau = 6\pi i \oint_{s=m_\tau} \frac{ds}{m_\tau^2} \left(1 - \frac{s}{m_\tau^2}\right) \left[ \left(1 + 2\frac{s}{m_\tau^2}\right) \Pi^{(T)}(s) + \Pi^{(L)} \right] \quad (3.2.3)$$

for the hadronic  $\tau$ -decay ratio. It is convenient to work with  $\Pi^{(T+L)}$ , which is connected to the vector/ axial-vector components of the correlator. Thus using eq. 3.1.10 in eq. 3.2.3 yields

$$R_\tau = 6\pi i \oint_{|s|=m_\tau} \frac{ds}{m_\tau^2} \left(1 - \frac{s}{m_\tau^2}\right)^2 \left[ \left(1 + 2\frac{s}{m_\tau^2}\right) \Pi^{(L+T)}(s) - \left(\frac{2s}{m_\tau^2}\right) \Pi^{(L)}(s) \right] \quad (3.2.4)$$

By introducing Cauchy's theorem we avoided low energies, which could lead to a breakdown of PT. The contour integral obtained is an important result as we are now able to theoretically evaluate the hadronic  $\tau$ -decay ratio at sufficiently large energy scales ( $m_\tau \approx 1.78 \text{ MeV}$ ) at which  $\alpha_s(m_\tau) \approx 0.33$  [37] is large enough to apply perturbation theory and the OPE. Obviously we would benefit from a contour integral over a bigger circumference, but  $\tau$ -decays are limited by the  $m_\tau$ . Nevertheless there are promising  $e^+e^-$  annihilation data, which yields valuable R-ratio values up to  $2 \text{ GeV}$  [7][29].

### 3.3 Pinched weights to avoid DVs

We are free to multiply eq. 3.2.2 by an analytic weight function  $\omega(s)$

$$\int_0^{m_\tau} \omega(s) \Pi(s) ds = \frac{i}{2} \oint_{s=m_\tau} \omega(s) \Pi(s) ds. \quad (3.3.1)$$

We can use this technique to suppress contributions for the two-point function close to the positive real axis by implementing so called pinched weights of the form

$$\omega(s) = \left(1 - \frac{s}{m_\tau^2}\right)^k, \quad (3.3.2)$$

where  $k$  is the degree of the pinched weight. The higher the degree the farther we operate from the critical positive real axis (see. ??), which suppresses the

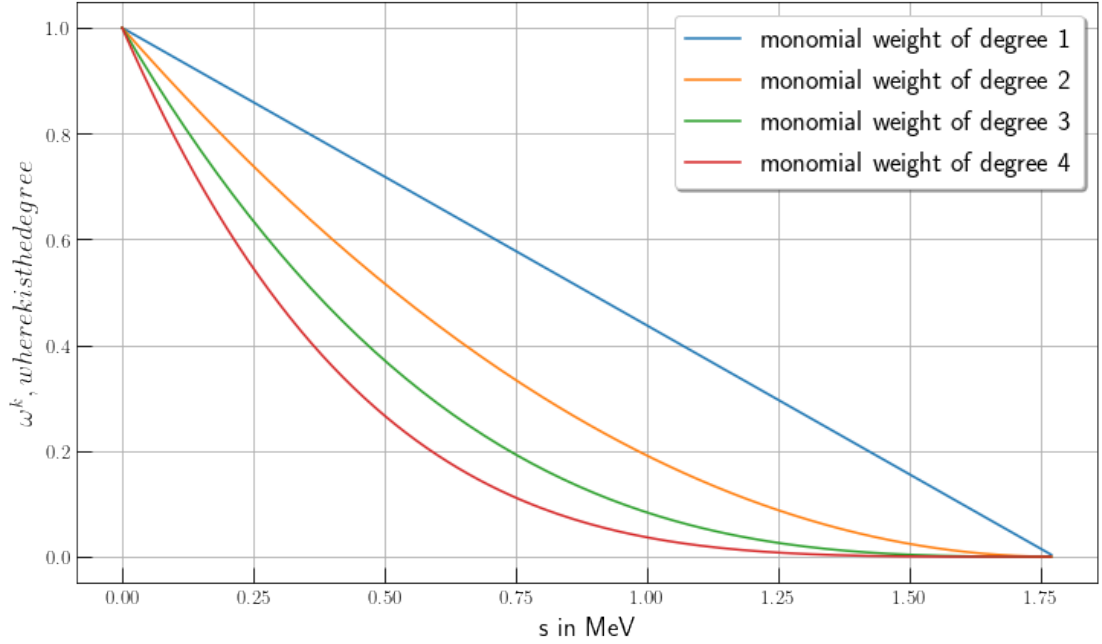


Figure 3.2: Monomial weights  $(1 - s/m_\tau^2)^k$  for degrees  $1 \rightarrow 4$ . We can see that weights of higher pinching decrease faster, which comes in handy if we want to suppress duality violations.

effects of duality violations. This pinching of second degree appears quite naturally. If we regard the include  $\tau$  – decay ratio [eq. 3.2.3](#), we note that for the transversal component we already have a double pinched weight, the *kinematic weight*

$$\omega_\tau(s) = \left(1 - \frac{s}{m_\tau^2}\right) \left(1 + 2\frac{s}{m_\tau^2}\right). \quad (3.3.3)$$

In general it is said that a double pinched weight is sufficient to neglect effects caused by duality violation.

We can also use different weights to control the dimensions of the OPE that contribute. The weights we are using have to be analytic, so that we can make use of Cauchy's theorem. Thus they can be represented as polynomials

$$\omega(x) = \sum_i a_i x^i, \quad (3.3.4)$$

every contributing monomial is responsible for a dimension of the OPE. Dimensions that are not represented in the weight polynomial do not contribute at all or are very suppressed as we will demonstrate now.



<b>monomial:</b>	$x^0$	$x^1$	$x^2$	$x^3$	$x^5$	$x^6$	$x^7$
<b>dimension:</b>	$D^{(2)}$	$D^{(4)}$	$D^{(6)}$	$D^{(8)}$	$D^{(10)}$	$D^{(12)}$	$D^{(14)}$

Table 3.1: List of monomial and their corresponding “active” dimensions in the OPE.

The residue of a monomial  $x^k$  is only different from 0 if its power  $k = -1$ :

$$\oint_C x^k dx = i \int_0^{2\pi} (e^{i\theta})^{k+1} d\theta = \begin{cases} 2\pi i & \text{if } k = -1, \\ 0 & \text{otherwise} \end{cases}. \quad (3.3.5)$$

Consequently if we exchange the kinematic weight of the include ratio [eq. 3.1.1](#) through a monomial and neglect all terms of no interest to us we can write

$$\begin{aligned} R(xm_\tau)|_{D=0,2,4,\dots} &= \oint_{|x|=1} \frac{x^k}{(xm_\tau)^{\frac{D}{2}}} C^D(xm_\tau) \\ &= \frac{1}{(m_\tau)^{\frac{D}{2}}} \oint_{|x|=1} x^{k-D/2} C^D(xm_\tau), \end{aligned} \quad (3.3.6)$$

where  $C^D$  are the  $D$ -dimensional Wilson coefficients. Thus combining [eq. 3.3.5](#) with [eq. 3.3.6](#) we see that only Dimension which fulfill

$$k - D/2 = -1 \implies D = 2(k + 1) \quad (3.3.7)$$

contribute to the OPE. For example the polynomial of the kinematic weight is given by

$$(1-x)^2(1+2x) = \underbrace{1}_{D=2} - 3 \underbrace{x^2}_{D=6} + 2 \underbrace{x^3}_{D=8} \quad (3.3.8)$$

where we underbraced the monomial and gave the active dimensions. A list of monomials and their corresponding Dimensions up to dimension 14 can be found in [table 3.1](#). This behavior enables us to bring out different dimensions of the OPE and suppress contributions of higher order ( $D \geq 10$ ) for which less is known.

## 3.4 RG invariance

The two-point function is not a physical quantity. It does not fulfill the RGE [eq. 2.1.10](#) and is thus dependent on the scale  $\mu$ . We can enhance the inclusive

ration eq. 3.1.1 making use of the **Adler function** defined as:

$$D^{(T+L)}(s) \equiv -s \frac{d}{ds} \Pi^{(T+L)}(s), \quad D^{(L)}(s) \equiv \frac{s}{m_\tau^2} \frac{d}{ds} (s \Pi^{(L)}(s)), \quad (3.4.1)$$

where we have two separate definitions: one for the transversal plus longitudinal contribution and one for solely longitudinal part. The two-point functions can now be replaced with the help of partial integration

$$\int_a^b u(x) V(x) dx = [u(x) V(x)]_a^b - \int_a^b u(x) v(x) dx. \quad (3.4.2)$$

We will do the computation for each of the two cases (T + L) and (L) separate. Starting by the transversal plus longitudinal contribution we get:

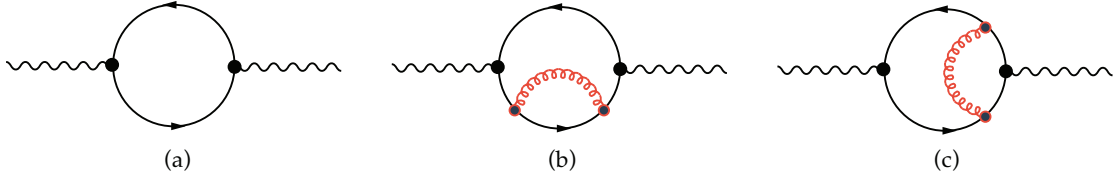
$$\begin{aligned} R_\tau^{(1)} &= \frac{6\pi i}{m_\tau^2} \oint_{|s|=m_\tau^2} \underbrace{\left(1 - \frac{s}{m_\tau^2}\right)^2}_{=u(x)} \underbrace{\left(1 + 2\frac{s}{m_\tau^2}\right) \Pi^{(L+T)}(s)}_{=V(x)} \\ &= \frac{6\pi i}{m_\tau^2} \left\{ \left[ -\frac{m_\tau^2}{2} \left(1 - \frac{s}{m_\tau^2}\right)^3 \left(1 + \frac{s}{m_\tau^2}\right) \Pi^{(L+T)}(s) \right]_{|s|=m_\tau^2} \right. \\ &\quad \left. + \oint_{|s|=m_\tau^2} \underbrace{-\frac{m_\tau^2}{2} \left(1 - \frac{s}{m_\tau^2}\right)^3}_{=u(x)} \underbrace{\left(1 + \frac{s}{m_\tau^2}\right) \frac{d}{ds} \Pi^{(L+T)}(s)}_{=v(x)} \right\} \\ &= -3\pi i \oint_{|s|=m_\tau^2} \frac{ds}{s} \left(1 - \frac{s}{m_\tau^2}\right)^3 \left(1 + \frac{s}{m_\tau^2}\right) \frac{d}{ds} D^{(L+T)} \end{aligned} \quad (3.4.3)$$

where we fixed the integration constant to  $C = -\frac{m_\tau^2}{2}$  in the second line and left the antiderivatives contained in the squared brackets untouched. If we parameterizing the integral appearing in the expression in the squared brackets we can derive that it vanishes:

$$\left[ -\frac{m_\tau^2}{2} \left(1 - e^{-i\phi}\right)^3 \left(1 + e^{-i\phi}\right) \Pi^{(L+T)}(m_\tau^2 e^{-i\phi}) \right]_0^{2\pi} = 0 \quad (3.4.4)$$

where  $s \rightarrow m_\tau^2 e^{-i\phi}$  and  $(1 - e^{-i \cdot 0}) = (1 - e^{-i \cdot 2\pi}) = 0$ . Repeating the same calculation for the longitudinal part yields

$$\begin{aligned} R_\tau^{(L)} &= \oint_{|s|=m_\tau^2} ds \left(1 - \frac{s}{m_\tau^2}\right)^2 \left(-\frac{2s}{m_\tau^2}\right) \Pi^{(L)}(s) \\ &= -4\pi i \oint \frac{ds}{s} \left(1 - \frac{s}{m_\tau^2}\right)^3 D^{(L)}(s) \end{aligned} \quad (3.4.5)$$



Consequently combining the two parts results in

$$R_\tau = -\pi i \oint_{|s|=m_\tau^2} \frac{ds}{s} \left(1 - \frac{s}{m_\tau^2}\right)^3 \left[ 3 \left(1 + \frac{s}{m_\tau^2} D^{(L+T)}(s) + 4 D^{(L)}(s) \right) \right]. \quad (3.4.6)$$

It is convenient to define  $x = s/m_\tau^2$  such that we can rewrite the inclusive ratio as

$$R_\tau = -\pi i \oint_{|s|=m_\tau^2} \frac{dx}{x} (1-x)^3 \left[ 3(1+x) D^{(L+T)}(m_\tau^2 x) + 4 D^{(L)}(m_\tau^2 x) \right]. \quad (3.4.7)$$

$$R_{\tau,V/A}^\omega = \frac{N_c}{2} S_{EW} |V_{ud}|^2 \left( 1 + \delta_\omega^{(0)} + \delta_\omega^{EW} + \delta_\omega^{DV_s} + \sum_{D \leq 2} \delta_{ud,\omega}^{(D)} \right) \quad (3.4.8)$$

### 3.5 The perturbative expansion

We will treat the correlator in the chiral limit for which the longitudinal components  $\Pi^L(s)$  vanish (see [eq. 3.1.11](#)) and the axial and vectorial contributions are equal. In the massless case we then can write the vector correlation function  $\Pi(s)$  as [\[4\]](#):

$$\Pi_V^{T+L}(s) = -\frac{N_c}{12\pi^2} \sum_{n=0}^{\infty} a_\mu^n \sum_{k=0}^{n+1} c_{n,k} L^k \quad \text{with} \quad L \equiv \ln \frac{-s}{\mu^2}. \quad (3.5.1)$$

The coefficient  $c_{n,k}$  up to two-loop order can be obtained by Feynman-diagram calculations. **add complete calculation** E.g. we can compare the zero-loop result of the correlator [\[26\]](#)

$$\Pi_{\mu\nu}^B(q^2) \Big|^{1\text{-loop}} = \frac{N_c}{12\pi^2} \left( \frac{1}{\hat{\epsilon}} - \log \frac{(-q^2 - i0)}{\mu^2} + \frac{5}{3} + \mathcal{O}(\epsilon) \right) \quad (3.5.2)$$

with [eq. 3.5.1](#) and extract the first two coefficients

$$c_{00} = -\frac{5}{3} \quad \text{and} \quad c_{01} = 1, \quad (3.5.3)$$

where  $\Pi_{\mu\nu}^B(q^2)$  is not renormalized<sup>1</sup>

The second loop can also be calculated by diagram techniques resulting in [5]

$$\Pi_V^{(1+0)}(s) \Big|^{2\text{-loop}} = -\frac{N_c}{12\pi^2} a_\mu \log\left(\frac{-s}{\mu^2}\right) + \dots \quad (3.5.4)$$

yielding  $c_{11} = 1$ .

Beginning from three loop diagrams the algebra becomes exhausting and one has to use dedicated algorithms to compute the higher loops. The third loop calculations have been done in the late seventies by [14, 19, 13]. The four loop evaluation have been completed a little more than ten years later by [23, 44]. The highest loop published, that amounts to  $\alpha_s^4$ , was published in 2008 [2] almost 20 years later.

Fixing the number of colors to  $N_c = 3$  the missing coefficients up to order four in  $\alpha_s$  read:

$$\begin{aligned} c_{2,1} &= \frac{365}{24} - 11\zeta_3 - \left(\frac{11}{12} - \frac{2}{3}\zeta_3\right) N_f \\ c_{3,1} &= \frac{87029}{288} - \frac{1103}{4}\zeta_3 + \frac{275}{6}\zeta_5 \\ &\quad - \left(\frac{7847}{216} - \frac{262}{9}\zeta_3 + \frac{25}{9}\zeta_5\right) N_f + \left(\frac{151}{162} - \frac{19}{27}\zeta_3\right) N_f^2 \\ c_{4,1} &= \frac{78631453}{20736} - \frac{1704247}{432}\zeta_3 + \frac{4185}{8}\zeta_3^2 + \frac{34165}{96}\zeta_5 - \frac{1995}{16}\zeta_7, \end{aligned} \quad (3.5.5)$$

where used the flavor number  $N_f = 3$  for the last line.

The 6-loop calculation has until today not been achieved, but Beneke and Jamin [4] used an educated guess to estimate the coefficient

$$c_{5,1} \approx 283 \pm 283. \quad (3.5.6)$$

Until now we have given the coefficients  $c_{n,k}$  with solely  $k = 1$ . This is due to the RGE, which relates coefficients with  $k$  different than one to the coefficients mentioned above. To make use of the RGE the correlator  $\Pi_V^{T+L}(s)$  needs to be a physical quantity, which can be achieved by rewriting it in terms of the Adler function (see. eq. 3.4.1) to:

$$D_V^{(T+L)} = -s \frac{d \Pi_V^{(T+L)}(s)}{ds} = \frac{N_c}{12\pi^2} \sum_{n=0}^{\infty} a_\mu^n \sum_{k=1}^{n+1} k c_{n,k} L^{k-1}, \quad (3.5.7)$$

---

<sup>1</sup>The term  $1/\hat{\epsilon}$ , which is of order  $o$  in  $\alpha_s$ , will be canceled by renormalization.

where we used  $dL^k/ds = k \ln(-s/\mu^2)^{k-1} (-1/\mu^2)$ . The Adler-function is physical quantity and has to fulfill the RGE [eq. 2.1.10](#):

$$-\mu \frac{d}{d\mu} D_V^{(T+L)} = -\mu \frac{d}{d\mu} \left( \frac{\partial}{\partial L} D_L + \frac{\partial}{\partial a_s} D_{a_s} \right) D_V^{T+L} = \left( 2 \frac{\partial}{\partial L} + \beta \frac{\partial}{\partial a_s} \right) D_V^{T+L} = 0, \quad (3.5.8)$$

where we defined the  $\beta$ -function in [eq. 2.1.11](#) and used  $dL/d\mu = -2/\mu$ . The RGE puts constraints on the  $c_{n,k}$ -coefficients for different  $k$ s, which are not independent anymore.

For example writing out the sum of the adler function to the second order in  $\alpha_s$  yields

$$D(s) = \frac{N_c}{12\pi^2} \left[ c_{01} + a_\mu (c_{11} + 2c_{12}L) + a_\mu^2 (c_{21} + 2c_{22}L + 3c_{23}L^2) \right]. \quad (3.5.9)$$

Then inserting [eq. 3.5.9](#) into the RGE

$$4a_\mu c_{12} + 2a_\mu^2 (2c_{22} + 6c_{23}L) + \beta_1 a_\mu^2 (c_{11} + 2c_{12}L) + \mathcal{O}(a_\mu^3) = 0 \quad (3.5.10)$$

lets us compare the coefficients order by order in  $\alpha_s$ . At order  $\alpha_\mu$  only the  $c_{12}$  term is present and has to be zero consequently. For  $\mathcal{O}(a_\mu^2 L)$  the only  $c_{23}$  exists ( $c_{12} = 0$ ) and has to vanish as well. Finally at  $\mathcal{O}(a)$  we can relate  $c_{22}$  with  $c_{11}$  resulting in:

$$c_{12} = 0, \quad c_{22} = \frac{\beta_1 c_{11}}{4} \quad \text{and} \quad c_{23} = 0. \quad (3.5.11)$$

or  $D(s)$  to the first order in  $\alpha_s$ . Implementing the newly obtained Adler-coefficients we can write out the adler function to the first order:

$$D(s) = \frac{N_c}{12\pi^2} \left[ c_{01} + c_{11} a_\mu \left( c_{21} - \frac{1}{2} \beta_1 c_{11} L \right) a_\mu^2 \right] + \mathcal{O}(a_\mu^3). \quad (3.5.12)$$

We have used the RGE to relate Adler-function coefficients and thus reduce its numbers. But as we will see in the following section the RGE gives us two different choices in the order of the computation of the perturbative contribution to the inclusive  $\tau$ -decay ratio.

### 3.5.1 Renormalization group summation

By making use of the RGE we have to decide about the order of mathematical operations we perform. As the perturbative contribution  $\delta^{(0)}$  is independent on the scale  $\mu$  we are confronted with two choices **fixed-order perturbation**

**theory (FOPT) or contour-improved perturbation theory.** Each of them yields a different result and is the main source of error in extracting the strong coupling from  $\tau$ -decays.

We can write the perturbative contribution  $\delta^{(0)}$  to  $R_\tau$  (see [eq. 3.4.8](#)) in the chiral limit, such that  $D^{(L)}$  vanishes as

$$\delta^{(0)} = \sum_{n=1}^{\infty} a_\mu^n \sum_{k=1}^n k c_{n,k} \frac{1}{2\pi i} \oint_{|x|=1} \frac{dx}{x} (1-x)^3 (1+x) \log \left( \frac{-M_\tau^2 x}{\mu^2} \right)^{k-1}, \quad (3.5.13)$$

where we inserted the expansion of  $D_V^{(T+L)}$  [eq. 3.4.1](#) into  $R_\tau$  [eq. 3.4.7](#). Keep in mind that the contributions from the vector and axial-vector correlator are identical in the massless case:

$$D^{(T+L)} = D_V^{(T+L)} + D_A^{(T+L)} = 2D_V^{(T+L)}. \quad (3.5.14)$$

In the following we will explain both the descriptions, starting by FOPT. By using the FOPT prescription we fix  $\mu^2 = m_\tau^2$  leading to

$$\delta_{\text{FO}}^{(0)} = \sum_{n=1}^{\infty} a(m_\tau^2)^n \sum_{k=1}^n k c_{n,k} J_{k-1} \quad (3.5.15)$$

where the contour integrals  $J_l$  are defined by

$$J_l \equiv \frac{1}{2\pi i} \oint_{|x|=1} \frac{dx}{x} (1-x)^3 (1+x) \log^l(-x). \quad (3.5.16)$$

The integrals  $J_l$  up to order  $\alpha_s^4$  are given by [\[4\]](#):

$$J_0 = 1, \quad J_1 = -\frac{19}{12}, \quad J_2 = \frac{265}{72} - \frac{1}{3}\pi^2, \quad J_3 = -\frac{3355}{288} + \frac{19}{12}\pi^2. \quad (3.5.17)$$

Using FOPT the strong coupling  $a(\mu)$ , which runs with the scale  $\mu$ , is fixed at  $a(m_\tau^2)$  and can be taken out of the closed-contour integral. Thus we solely to integrate over the logarithms  $\log(-s/m_\tau^2)$ .

Using CIPT we can sum the logarithms by setting the scale to  $\mu^2 = -m_\tau^2 x$  in [eq. 3.5.13](#), resulting in:

$$\delta_{\text{CI}}^{(0)} = \sum_{n=1}^{\infty} c_{n,1} J_n^a(m_\tau^2), \quad (3.5.18)$$

where the contour integrals  $J_l$  are defined by

$$J_n^a(m_\tau^2) \equiv \frac{1}{2\pi i} \oint_{|x|=1} \frac{dx}{x} (1-x)^3 (1+x) a^n(-m_\tau^2 x). \quad (3.5.19)$$

All logarithms vanish except the ones for  $k = 1$ :

$$\log(1)^{k-1} = \begin{cases} 1 & \text{if } k = 1, \\ 0 & k \neq 1 \end{cases} \quad (3.5.20)$$

which selects adler function coefficients  $c_{n,1}$  with a fixed  $k = 1$ . Handling the logarithms left us with the integration of  $\alpha_s(-m_\tau^2 x)$  over the closed-contour  $\oint_{|x|=1}$ , which now depends on the integration variable  $x$ . In general we have to decide if we want to perform a contour integration with a constant coupling constant and variable logarithms (FOPT) or “constant logarithms” and a running coupling (CIPT).

To emphasize the differences in both approaches we can calculate the perturbative contribution  $\delta^{(0)}$  to  $R_\tau$  for the two different prescriptions yielding [4]

$$\begin{aligned} & \alpha_s^2 \quad \alpha_s^2 \quad \alpha_s^3 \quad \alpha_s^4 \quad \alpha_s^5 \\ \delta_{\text{FO}}^{(0)} &= 0.1082 + 0.0609 + 0.0334 + 0.0174(+0.0088) = 0.2200(0.2288) \end{aligned} \quad (3.5.21)$$

$$\delta_{\text{CI}}^{(0)} = 0.1479 + 0.0297 + 0.0122 + 0.0086(+0.0038) = 0.1984(0.2021). \quad (3.5.22)$$

The series indicate, that CIPT converges faster and that both series approach a different value. This discrepancy represents currently the biggest theoretical uncertainty while extracting the strong coupling  $\alpha_s$ .

As today we do not know if FOPT or CIPT is the correct approach of measuring  $\alpha_s$ . Therefore there are currently three ways of stating results:

- Quoting the average of both results.
- Quoting the CIPT result.
- Quoting the FOPT result.

We follow the approach of Beneke and Jamin [4] who have shown advantages of FOPT over CIPT.

### 3.6 Non-Perturbative OPE Contribution

The perturbative contribution to the Sum-Rule, that we have seen so far, is the dominant one. With

$$\begin{aligned} R_\tau^{\text{FOPT}} &= \\ R_\tau^{\text{CIPT}} &= \end{aligned} \quad (3.6.1)$$

The NP vs perturbative contributions can be varied by chosen different weights than  $\omega_\tau$ .

#### 3.6.1 Dimension four

For the OPE contributions of dimension four we have to take into account the terms with masses to the fourth power  $m^4$ , the quark condensate multiplied by a mass  $m\langle\bar{q}q\rangle$  and the gluon condensate  $\langle GG\rangle$ . The resulting expression can be taken from the appendix of [36], yielding:

$$D_{ij}^{(L+T)}(s)\Big|_{D=4} = \frac{1}{s^2} \sum_n \Omega^{(1+0)}(s/\mu^2) a^n, \quad (3.6.2)$$

where

$$\begin{aligned} \Omega_n^{(1+0)}(s/\mu^2) &= \frac{1}{6} \langle aGG \rangle p_n^{(L+T)}(s/\mu^2) + \sum_k m_k \langle \bar{q}_k q_k \rangle r_n^{(L+T)}(s/\mu^2) \\ &+ 2 \langle m_i \bar{q}_i q_i + m_j \bar{q}_j q_j \rangle q_n^{(L+T)}(s/\mu^2) \pm \frac{8}{3} \langle m_j \bar{q}_i q_i + m_i \bar{q}_j q_j \rangle t_n^{(L+T)} \\ &- \frac{3}{\pi^2} (m_i^4 + m_j^4) h_n^{(L+T)}(s/\mu^2) \mp \frac{5}{\pi^2} m_i m_j (m_i^2 + m_j^2) k_n^{(L+T)}(s/\mu^2) \\ &+ \frac{3}{\pi^2} m_i^2 m_j^2 g_n^{(L+T)}(s/\mu^2) + \sum_k m_{kj}^4 \dot{r}_n^{(L+T)}(s/\mu^2) + 2 \sum_{k \neq l} m_k^2 m_l^2 u_n^{(L+T)}(s/\mu^2) \end{aligned} \quad (3.6.3)$$

The perturbative expansion coefficients are known to  $\mathcal{O}(\alpha^2)$  for the condensate contributions,

$$\begin{aligned} p_0^{(L+T)} &= 0, & p_1^{(L+T)} &= 1, & p_2^{(L+T)} &= \frac{7}{6}, \\ r_0^{(L+T)} &= 0, & r_1^{(L+T)} &= 0, & r_2^{(L+T)} &= -\frac{5}{3} + \frac{8}{3}\zeta_3 - \frac{2}{3}\log(s/\mu^2), \\ q_0^{(L+T)} &= 1, & q_1^{(L+T)} &= -1, & q_2^{(L+T)} &= -\frac{131}{24} + \frac{9}{4}\log(s/\mu^2) \\ t_0^{(L+T)} &= 0, & t_1^{(L+T)} &= 1, & t_2^{(L+T)} &= \frac{17}{2} + \frac{9}{2}\log(s/\mu^2). \end{aligned} \quad (3.6.4)$$



while the  $m^4$  terms have been only computed to  $\mathcal{O}(\alpha)$

$$\begin{aligned}
 h_0^{(L+T)} &= 1 - 1/2 \log(s/\mu^2), & h_1^{(L+T)} &= \frac{25}{4} - 2\zeta_3 - \frac{25}{6} \log(s/\mu^2) - 2 \log(s/\mu^2)^2, \\
 k_0^{(L+T)} &= 0, & k_1^{(L+T)} &= 1 - \frac{2}{5} \log(s/\mu^2), \\
 g_0^{(L+T)} &= 1, & g_1^{(L+T)} &= \frac{94}{9} - \frac{4}{3} \zeta_3 - 4 \log(s/\mu^2), \\
 j_0^{(L+T)} &= 0, & j_1^{(L+T)} &= 0, \\
 u_0^{(L+T)} &= 0, & u_2^{(L+T)} &= 0.
 \end{aligned} \tag{3.6.5}$$

### 3.6.2 Dimension six and eight

Our application of dimension six contributions is founded in [9] and has previously been calculated beyond leading order by [30]. The operators appearing are the masses to the power six  $m^6$ , the four-quark condensates  $\langle \bar{q} q \bar{q} q \rangle$ , the three-gluon condensates  $\langle g^3 G^3 \rangle$  and lower dimensional condensates multiplied by the corresponding masses, such that in total the mass dimension of the operator will be six. As there are too many parameters to be fitted with experimental data we have to omit some of them, starting with the three-gluon condensate, which does not contribute at leading order. The four-quark condensates known up to  $\mathcal{O}(\alpha^2)$ , but we will make use of the *vacuum saturation approach* [4, 9, 43] to express them in quark, anti-quark condensates  $\langle q \bar{q} \rangle$ . In our work we take the simplest approach possible: Introducing an effective dimension six coefficient  $\rho_{V/A}^{(6)}$  divided by the appropriate power in  $s$

$$D_{ij,V/A}^{(1+0)} \Big|_{D=6} = 0.03 \frac{\rho_{V/A}^{(6)}}{s^3} \tag{3.6.6}$$

As for the dimension eight contribution the situation is not better than the dimension six one we keep the simplest approach, leading to

$$D_{ij,V/A}^{(1+0)} \Big|_{D=8} = 0.04 \frac{\rho_{V/A}^{(8)}}{s^4}. \tag{3.6.7}$$

### 3.6.3 Duality Violations

## 3.7 Experiment

The  $\tau$ -decay data we use to perform our QCD-analysis is from the **ALEPH** experiment. The ALEPH experiment was located at the large-electron-positron (LEP) collider at CERN laboratory in Geneva. LEP started producing particles in 1989 and was replaced in the late 90s by the large-hadron-collider, which makes use of the same tunnel of 27km circumference. The data produced within the experiment is still maintained by former ALEPH group members under led by M. Davier, which have performed regular updates on the data-sets [18, 15, 40].

The measured spectral functions for the Aleph data are defined in [16] and given for the transverse and longitudinal components separately:

$$\rho_{V/A}^{(T)}(s) = \frac{m_\tau^2}{12|V_{ud}^2|S_{EW}} \frac{\mathcal{B}(\tau^- \rightarrow V^-/A^- \nu_\tau)}{\mathcal{B}(\tau^- \rightarrow e^- \bar{\nu}_e \nu_\tau)} \times \frac{dN_{V/A}}{N_{V/A} ds} \left[ \left(1 - \frac{s}{m_\tau^2}\right)^2 \left(1 + \frac{2s}{m_\tau^2}\right) \right]^{-1} \quad (3.7.1)$$

$$\rho_A^{(L)}(s) = \frac{m_\tau^2}{12|V_{ud}^2|S_{EW}} \frac{\mathcal{B}(\tau^- \rightarrow \pi^-(K^-) \nu_\tau)}{\mathcal{B}(\tau^- \rightarrow e^- \bar{\nu}_e \nu_\tau)} \times \frac{dN_A}{N_A ds} \left(1 - \frac{s}{m_\tau^2}\right)^{-2}.$$

$$\mathcal{B}_e = \dots \quad (3.7.2)$$

$$R_{\tau,V/A} = \frac{\mathcal{B}_{V/A,\tau}}{\mathcal{B}_e} \quad (3.7.3)$$

The data relies on a separation into vector and axial-vector channels. In the case of the Pions this can be achieved via counting. The vector channel is characterised by a negative parity, whereas the axial-vector channel has positive parity. A quark has by definition positive parity, thus an anti-quark has a negative parity. A meson, like the Pion particle, is a composite particle consisting of an quark an anti-quark. Consequently a single Pion carries negative parity, an even number of Pions carries positive parity and an odd number of Pions

carries negative parity:

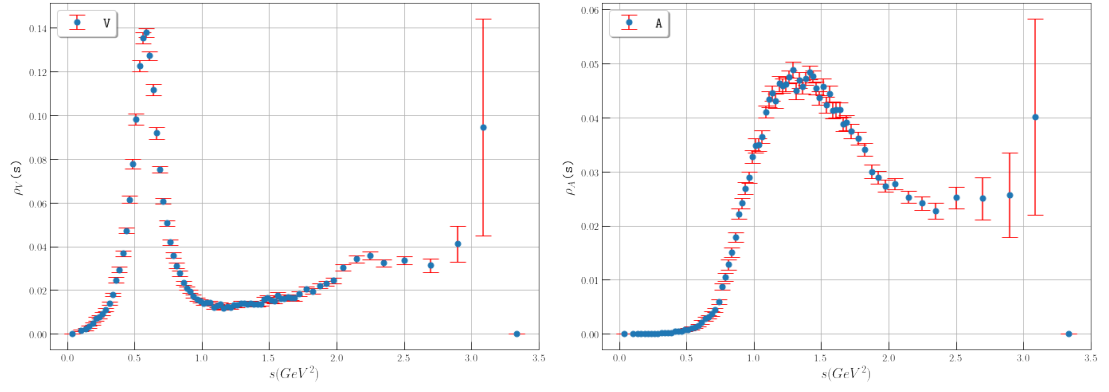
$$n \times \pi = \begin{cases} \text{vector} & \text{if } n \text{ is even,} \\ \text{axial-vector} & \text{otherwise} \end{cases} . \quad (3.7.4)$$

The contributions to the vector and axial channel can be seen in [figure](#). The dominant modes in the vector case are [\[17\]](#)  $\tau^- \rightarrow \pi^- \pi^0 \nu_\tau$  and the  $\tau^- \rightarrow \pi^- \pi^- \pi^+ \pi^0 \nu_\tau$ . The first of these is produced by the  $\rho(770)$  meson, which is contrary to the pions carries angular momentum of one, which is also clearly visible as peak around 770 GeV in [figure vector](#). The dominant modes in the axial-vector case are  $\tau^- \rightarrow \pi^- \nu_\tau$ ,  $\tau^- \rightarrow \pi^- \pi^0 \pi^0 \nu_\tau$  and  $\tau^- \rightarrow \pi^- \pi^- \pi^+ \nu_\tau$ . Here the three pion final states stem from the  $a_1^-$ -meson, which is also clearly visible as a peak in [figure](#).

wavy  $\Rightarrow$  DV OPE cannot reproduce suppressed in VpA regions below 1.5 GeV  
can still not be applied

The different inclusive  $\tau$ -decay ratios are then given by

$$R_{\tau,V} = \dots \quad (3.7.5)$$



(a) A gull

(b) A mouse

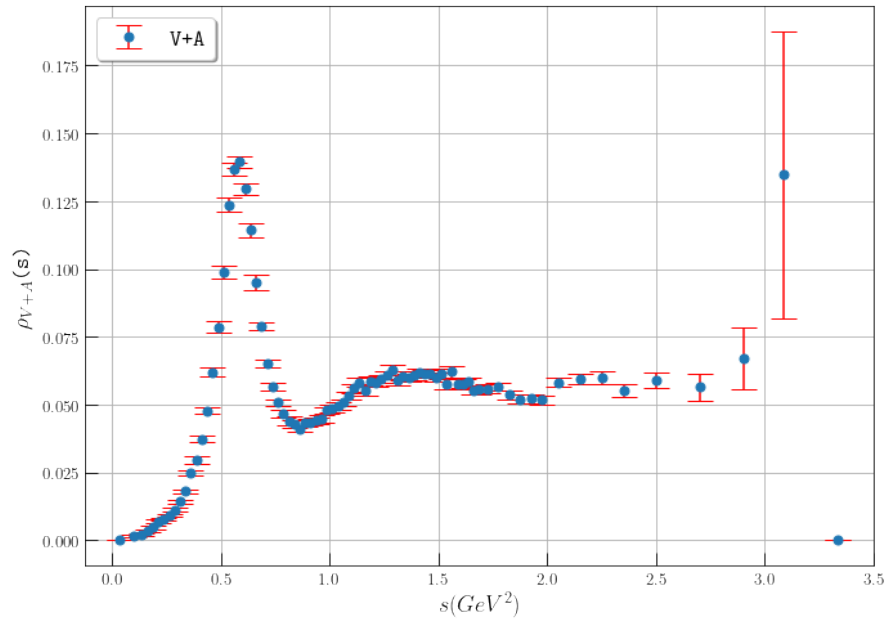


Figure 3.3: Pictures of animals

# Measuring the strong coupling

## 4.1 Fits

In the following we will perform fits to determine  $\alpha_s$  at the  $m_\tau^2$ -scale. The fits are separated corresponding to the used weight. Every weight contains multiple fits for different  $s_0$ -momenta. We will start with the kinematic weight, which appears naturally in the inclusive  $\tau$ -decay ratio [eq. 3.1.1](#) and has the best fitting characteristics of all weights we have used.

### 4.1.1 Kinematic weight: $\omega_\tau(x) \equiv (1-x)^2(1+2x)$

The kinematic weight is defined as  $\omega(x) = (1-x)^2(1+2x)$ . It is a double pinched, polynomial weight-function that contains the unity and does not contain a term proportional to  $x$ , which makes it an optimal weight [\[3\]](#). As a doubled pinched weight it should have a good suppression of DV-contributions and its polynomial contains terms proportional to  $x^2$  and  $x^3$ , which makes it sensitive to the dimension six and eight OPE contributions. The fits have been performed within the framework of FOPT for different numbers of  $s_0$ . The momentum sets are characterised by its lowest energy  $s_{\min}$ . We fitted values down to 1.5 GeV. Going to lower energies is questionable due to the coupling constant becoming too large, which implies a breakdown of PT and appearing DVs. Furthermore it bears the risk to be affected by the  $\rho(770)$  and  $a_1$  peaks in the vector and axial-vector spectral function, which we cannot model within the framework of the OPE. For the fitting-parameters  $\alpha_s, c_6$  and

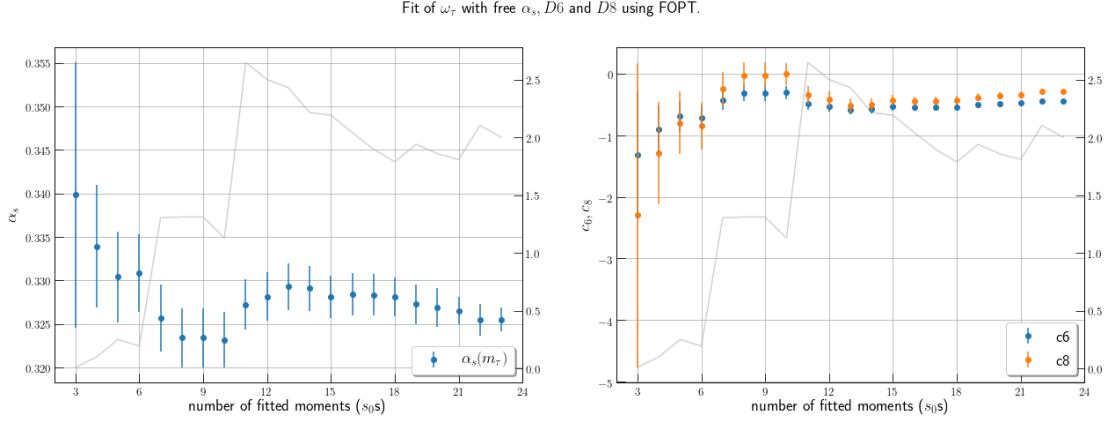


Figure 4.1: Fitting values of  $\alpha_s(m_\tau^2)$ ,  $c_6$  and  $c_8$  for the kinematic weight  $\omega(x) = (1-x)^2(1+2x)$  using FOPT for different  $s_{\min}$ . The left graph plots  $\alpha_s(m_\tau^2)$  for different numbers of used  $s_0s$ . The right plot contains the dimension six and eight contributions to the OPE. Both plots have in grey the  $\chi^2$  per degree of freedom (dof).

$c_8$  we have given the results in [table 4.1](#) and graphically in [fig. 4.1](#).

$s_{\min}$	# $s_0s$	$\alpha_s(m_\tau^2)$	$c_6$	$c_8$	$\chi^2/\text{dof}$
1.950	10	0.3232(32)	-0.31(11)	-0.01(18)	1.13
2.000	9	0.3234(34)	-0.32(12)	-0.03(21)	1.31
2.100	8	0.3256(38)	-0.43(15)	-0.25(28)	1.30
2.200	7	0.3308(44)	-0.72(20)	-0.85(38)	0.19
2.300	6	0.3304(52)	-0.69(25)	-0.80(50)	0.25
2.400	5	0.3339(70)	-0.91(39)	-1.29(83)	0.10
2.600	4	0.3398(15)	-1.3(1.0)	-2.3(2.5)	0.01

Table 4.1: Table of our fitting values of  $\alpha_s(m_\tau^2)$ ,  $c_6$  and  $c_8$  for the kinematic weight  $\omega(x) = (1-x)^2(1+2x)$  using FOPT ordered by increasing  $s_{\min}$ . The errors are given in parenthesis after the observed value.

We only display the fits for  $s_{\min}$  larger than 1.95 GeV as fits with higher  $s_{\min}$  have a too large  $\chi^2$  (larger than two). We achieved six good fits with a  $\chi^2$  per dof less or close to one, which we divided into two groups:

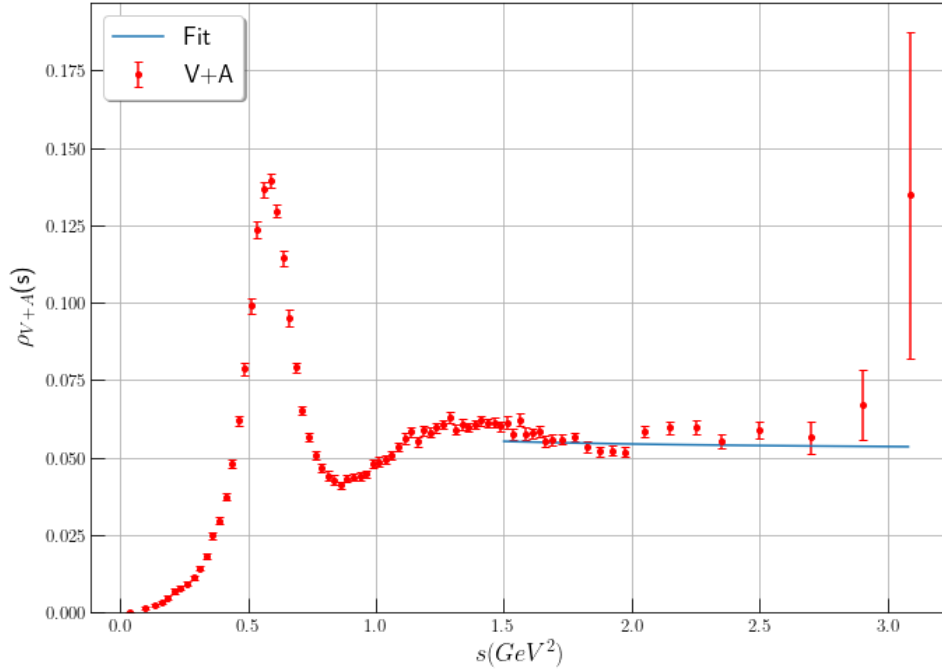


Figure 4.2: test

- Fits with **5-7** momenta have  $\chi^2$  per DOF larger than one and means of  $\alpha(m_\tau^2) = 0.3317(33)$ ,  $c_6 = -0.77(17)$  and  $c_8 = -0.98(35)$ , where we propagated the uncertainty. We have excluded the momentum containing four  $s_0$ s, because its  $\chi^2$  is too low and its errors are too large, which is because we have to fix three variables for only four data points.
- Fits with **8-10** momenta have small  $\chi^2$  per DOF values and lower means for the strong coupling  $\alpha(m_\tau^2) = 0.3241(20)$  but the OPE contributions are higher  $c_6 = -0.350(75)$  and  $c_8 = -0.09(12)$ .

The values for the less momenta are preferred by us due to two reasons. First below energies of 2.2 GeV we have to face the problematic influence of increasing resonances. Second, we will see, that the values obtained from the lower moment fits are more compatible with our other fits series. For both, the momenta sets, we see a good convergence of the OPE.

We further tested the stability of the dimension six and eight contributions to the OPE within the same fit series but for a fixed value of the strong coupling

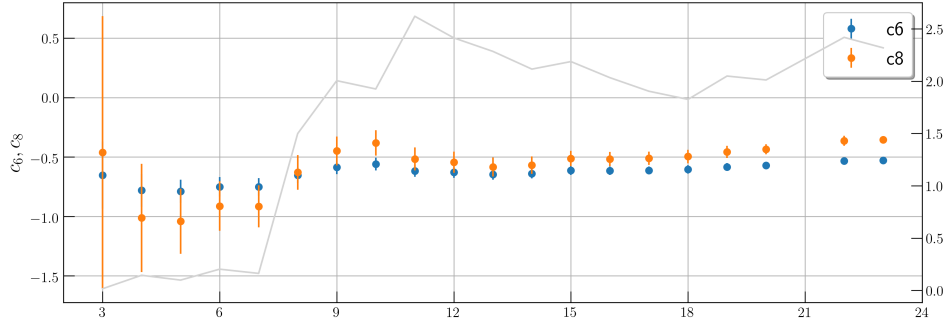


Figure 4.3

to our previous averaged result  $\alpha_s(m_\tau^2) = 0.3179$ . The fits have been plotted in [fig. 4.3](#) and show good stability. The values for  $c_6$  and  $c_8$  are larger than the values given in our final results from [table 4.1](#). This is explained with a smaller contribution from the strong coupling ( $\alpha_s$  is smaller), which has to be compensated by larger OPE contributions.

Due to the good results we will try to argue in favour of the values obtained by the lower momenta:

$$\alpha_s(m_\tau^2) = 0.3317(33), \quad c_6 = -0.77(17) \quad \text{and} \quad c_8 = -0.98(35). \quad (4.1.1)$$

#### 4.1.2 Cubic weight: $\omega_{\text{cube}}(x) \equiv (1-x)^3(1+3x)$

To further consolidate the results from the kinematic weight, we test a weight of higher pinching, which is known to suppress DV more than a double pinched weight would do. Consequently, any differences to the previous fit could indicate a problem with the DV treatment. Our *cubic* weight will be triple pinched and optimal, as the kinematic weight is double pinched and we do not want any problematic contributions proportional to  $x$ . Thus we define the *cubic weight* as  $\omega_{\text{cube}}(x) \equiv (1-x)^3(1+3x)$ . It is due to its polynomial structure sensitive to the dimensions six, eight and ten contributions of the OPE, which yields one more parameter to fit than with the kinematic weight  $\omega_\tau$ . The some good, selected fits, by  $\chi^2$  per DOF, can be seen in [table 4.2](#) and graphically in [section 4.1.2](#). As with the kinematic weight we get two different sets of value:

- The fits with **9, 10 and 11** momenta have a too high  $\chi^2$ , but are compa-



$s_{\min}$	$\#s_0s$	$\alpha_s(m_\tau^2)$	$c_6$	$c_8$	$c_{10}$	$\chi^2/\text{dof}$
1.900	11	0.3249(29)	-0.280(20)	-0.088(21)	0.088(55)	1.58
1.950	10	0.3237(26)	-0.232(25)	0.005(42)	0.275(93)	1.67
2.000	9	0.3228(26)	-0.196(27)	0.075(28)	0.420(56)	1.96
2.100	8	0.3302(40)	-0.52(11)	-0.58(22)	-1.00(45)	0.43
2.200	7	0.3312(43)	-0.56(12)	-0.68(23)	-1.23(50)	0.55
2.300	6	0.336(11)	-0.78(47)	-1.17(98)	-2.38(22)	0.29
2.400	5	0.3330(96)	-0.63(47)	-0.82(10)	-1.51(26)	0.48

Table 4.2: Table of our fitting values of  $\alpha_s(m_\tau^2)$ ,  $c_6$ ,  $c_8$  and  $c_{10}$  for the cubic weight  $\omega(x) = (1-x)^3(1+3x)$  using FOPT ordered by increasing  $s_{\min}$ . The errors are given in parenthesis after the observed value.

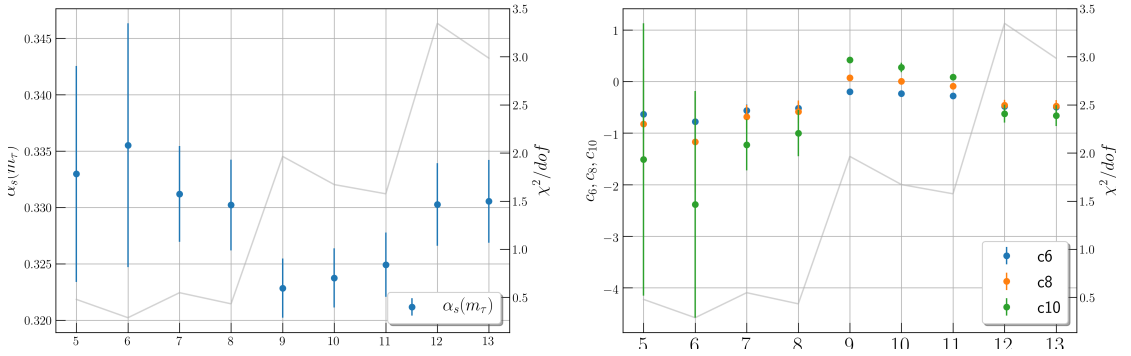


table to our the upper entries of the kinematic weight table [table 4.1](#). As with the kinematic weight the  $s_{\min}$  seems to be affected by lower resonances.

- The fits with **5,6,7 and 8** have a better  $\chi^2$  per DOF value and are in good agreement with the corresponding fits of the kinematic weight. The averaged value with its propagated errors read:  $\alpha_s(m_\tau^2) = 0.332478(61)$ ,  $c_6 = -0.622(12)$ ,  $c_8 = -0.815(55)$  and  $c_{10} = -1.5(3.1)$ .

We furthermore found that the OPE is converging, but not as good as for the kinematic weight. The values of  $|\delta^{(8)}|$  is only half as large as  $|\delta^{(8)}|$ . The values of the lower momentum count are in high agreement with the ones obtained from the kinematic weight. The conclusions that we take from the *cubic weight* are that the kinematic weight, with its double pinching, should sufficiently suppress any contributions from DVs. If DV would have an effect on the kinematic weight, we should have seen an improvement of the fits with the *cubic weight*, due to its triple pinching, which is not the case.

#### 4.1.3 Quartic weight: $\omega(x) \equiv (1-x)^4(1+4x)$

To include an even higher pinching of four and to compare the previously obtained value for the dimension ten OPE contribution we performed fits with the *quartic weight* defined as  $\omega(x) \equiv (1-x)^4(1+4x)$ , which also fulfils the definition of an optimal weight [3]. Unfortunately the fits only converged for  $s_{\min} = 2 \text{ GeV}$  (nine  $s_0$ s moment combination). The results for , with a  $\chi^2$  per DOF of 0.67 are given by:

$$\begin{aligned} \alpha_s(m_\tau^2) &= 0.3290(11), & c_6 &= -0.3030(46), & c_8 &= -0.1874(28), \\ c_{10} &= 0.3678(45) & \text{and} & & c_{12} &= -0.4071(77) \end{aligned} \tag{4.1.2}$$

Due to the problematic of the fitting routing, which is caused by too many OPE contributions fitted simultaneously, we will discard the fitting results for the quartic weight.

$s_{\min}$	$\#s_0s$	$\alpha_s(m_\tau^2)$	$c_8$	$\chi^2/\text{dof}$
2.200	7	0.3214(49)	-1.01(39)	0.41
2.300	6	0.3227(57)	-1.18(54)	0.46
2.400	5	0.3257(67)	-1.58(74)	0.39
2.600	4	0.325(10)	-1.54(1.53)	0.58
2.800	3	0.326(21)	-1.69(4.03)	1.17

Table 4.3: Table of our fitting values of  $\alpha_s(m_\tau^2)$ , and  $c_8$  for the single pinched third power monomial weight  $\omega(x) = 1 - x^3$  using FOPT ordered by increasing  $s_{\min}$ . The errors are given in parenthesis after the observed value.

#### 4.1.4 Third power monomial: $\omega_{m3}(x) \equiv 1 - x^3$

To study the behaviour of the DV and the higher order OPE contributions of dimension eight and ten we further included two optimal, single pinched weights. The first one is defined as  $\omega_{m3}(x) \equiv 1 - x^3$  and contains a single third power monomial and is consequently sensitive to dimension eight contributions from the OPE. Our fitting results can be taken from [table 4.3](#). The  $\chi^2$  per DOF is like in the  $\omega_\tau$  and  $\omega_{\text{cubic}}$  fits good for  $s_{\min} \leq 2.2 \text{ GeV}$ , but jumps to values  $\chi^2/\text{dof} > 1.4$  for smaller  $s_{\min}$ . This is, as before, explained through resonances that appear in lower energies. Due to the good  $\chi^2$  and the internally compatible fitting values we averaged over all rows except the last one of [table 4.3](#). The last row, at  $s_{\min} = 2.8 \text{ GeV}$  has only one DOF and thus high errors. The averaged values are thus given by

$$\alpha(m_\tau^2) = 0.32382(42) \quad \text{and} \quad c_8 = -1.33(67). \quad (4.1.3)$$

We note that the strong coupling is smaller as our expected values from the kinematic weight ??, but the dimension eight contribution is in good agreement. The strong coupling from the monomial weight to third order seems to be in better agreement with the 8-10 momenta used in the kinematic fits, whereas the dimension eight contributions agrees more with the 4-7 momenta fits.

We have made use of a single pinched weight and discovered that the fitting

$s_{\min}$	$\#s_0s$	$\alpha_s(m_\tau^2)$	$c_{10}$	$\chi^2/\text{dof}$
2.200	7	0.3203(48)	-1.64(77)	0.42
2.300	6	0.3216(56)	-2.01(1.13)	0.47
2.400	5	0.3247(66)	-2.98(1.62)	0.39
2.600	4	0.324(10)	-2.86(3.69)	0.58
2.800	3	0.325(20)	-3.43(10.74)	1.17

Table 4.4: Table of our fitting values of  $\alpha_s(m_\tau^2)$  and  $c_{10}$  for the single pinched fourth power monomial weight  $\omega(x) = 1 - x^4$  using FOPT ordered by increasing  $s_{\min}$ . The errors are given in parenthesis after the observed value.

result is not completely compatible with our previous fitting results. Consequently weights with a pinching less than two are affected by DV and should not be used to determine the strong coupling.

#### 4.1.5 Fourth power monomial: $\omega_{m4}(x) \equiv 1 - x^4$

We already analysed the cubic and quartic weights, which depend on the dimension ten OPE contribution, in [section 4.1.2](#) and [section 4.1.3](#) correspondingly. Now, even with the visible DV for fourth power monomial  $\omega_{m4} \equiv 1 - x^4$  to study another single pinched moment and the dimension ten OPE contribution. The results of the are given in ???. The fitting behaviour is very similar to the third power monomial (??) and we will directly cite our obtained results:

$$\alpha_s(m_\tau^2) = 0.32277(40) \quad \text{and} \quad c_{10} = -2.4(3.6). \quad (4.1.4)$$

As before the values for the strong coupling are lower than the ones obtained by the kinematic weight fit. Furthermore the error on the tenth dimension contribution of the OPE are too huge, although the huge errors makes it compatible with all previous results. All in all the usage of the single pinched fourth power monomial weight is questionable and does not deliver any additional insights.

### 4.1.6 Pich's Optimal Moments [37]

Next to the previously mentioned *optimal weights* from Beneke and Jamin [3] there are *optimal moments* introduced by Pich [31]. Combinations of these optimal moments have been widely used by the ALEPH collaboration to perform QCD analysis on the Large electron-positron collider (LEP). These moments include the for FOPT problematic proportional term in  $x$  [3], thus we will perform additional fits in the Borel-sum.

$$\omega_{(n,m)}(x) = (1-x)^n \sum_{k=0}^m (k+1)x^k \quad (4.1.5)$$

$$\omega(x) = (1-x)^2$$

$s_{\min}$	$\#s_0s$	$\alpha_s(m_\tau^2)$	aGGInv	$c_6$	$\chi^2/\text{dof}$
2.200	7	0.3401(57)	-0.0185(52)	0.220(88)	0.73
2.300	6	0.3383(68)	-0.0165(67)	0.26(12)	0.89
2.400	5	0.3450(93)	-0.0243(99)	0.10(17)	0.71
2.600	4	0.337(16)	-0.014(18)	0.36(45)	0.98

Table 4.5: Table of our fitting values of  $\alpha_s(m_\tau^2)$ , aGGInv and  $c_6$  for the triple pinched optimal weight  $\omega^{(2,0)}(x) = (1-x)^2$  using FOPT ordered by increasing  $s_{\min}$ . The errors are given in parenthesis after the observed value.

$$\omega(x) = (1 - x)^3$$

$s_{\min}$	$\#s_0S$	$\alpha_s(m_t^2)$	aGGInv	$c_6$	$c_8$	$\chi^2/\text{dof}$
1.900	11	0.34281(92)	-0.01473(73)	-0.103(22)	-0.534(46)	1.52
1.950	10	0.34154(99)	-0.01304(61)	-0.050(17)	-0.389(44)	1.42
2.000	9	0.33985(81)	-0.01124(43)	0.002(10)	-0.242(26)	1.59
2.100	8	0.3480(47)	-0.0201(36)	-0.264(89)	-1.03(28)	0.31
2.200	7	0.3483(23)	-0.0204(41)	-0.27(15)	-1.05(40)	0.41
2.300	6	0.3522(64)	-0.0249(62)	-0.42(18)	-1.51(57)	0.29
2.400	5	0.3480(89)	-0.0199(100)	-0.25(33)	-0.96(10)	0.39

Table 4.6: Table of our fitting values of  $\alpha_s(m_t^2)$ , aGGInv,  $c_6$  and  $c_8$  for the optimal weight  $\omega^{(3,0)}(x) = (1 - x)^3$  using FOPT ordered by increasing  $s_{\min}$ . The errors are given in parenthesis after the observed value.

weight	$s_{\min}$	$\alpha_s(m_\tau^2)$	aGGInv	$c_6$	$c_8$	$c_{10}$	$\chi^2/\text{dof}$
$\omega_{\text{kin}}$	2.2	0.3308(44)	-	-0.72(20)	-0.85(38)	-	0.19
$\omega_{\text{cube}}$	2.1	0.3302(40)	-	-0.52(11)	-0.58(22)	-1.00(45)	0.43
$\omega_{3,0}^*$	2.1	0.3239(30)	-0.2125(26)	-0.627(87)	-0.74(17)	-	0.46
$\omega_{\text{quartic}}$	2.0	0.3290(11)	-	-0.3030(46)	-0.1874(28)	0.3678(45)	0.67
$\omega_{\text{m3}}$	2.2	0.3214(49)	-	-	-1.01(39)	-	0.41
$\omega_{\text{m4}}$	2.2	0.3203(48)	-	-	-	-1.64(77)	0.42
$\omega_{2,0}$	2.2	0.3401(57)	-0.0185(52)	0.220(88)	-	-	0.73
$\omega_{3,0}$	2.1	0.3480(47)	-0.0201(36)	-0.264(89)	-1.03(28)	-	0.31

Table 4.7: Table of the best fits (selected by  $\chi^2/\text{dof}$  and compatibility of the fitting values) for each weight including at least the strong coupling  $\alpha_s(m_\tau^2)$  as a fitting variable. All fits have been performed using `FORT`, except weights marked with a star  $\omega^*$ , which have been fitted using the *Borel sum*.

#### 4.1.7 Comparison

To create an overview of our previous results we have gathered the most compatible rows by hand. These are shown in [table 4.7](#), which is composed of two parts:

- The upper three rows represent fits we found to have good properties for determining the strong coupling.
- The lower five rows are problematic fits due to too many OPE contributions, too low pinching or to terms proportional to  $x$ .

We have found that the kinematic weight is in excellent agreement with the cubic  $\omega_{\text{cube}}$  and Pich’s optimal weight  $\omega_{3,0}$ , fitted using the borel model. The fitted parameters from the kinematic weight ( $\alpha_s, c_6$  and  $c_8$ ) are all within error ranges and thus compatible. One fact that has to be investigated is the negative appearing sign for the gluon-condensate from the borel-sum of  $\omega_{3,0}$ .

### 4.1.8 Toni Pich 2006

#### 4. ALEPH determination

Toni built moments with five different weights:

$$\omega_{kl}(x) = (1-x)^{2+k}x^l(1+x) \quad \text{with} \quad (k,l) = (0,0), (1,0), (1,1), (1,2), (1,3) \quad (4.1.6)$$

He always fitted weight combinations, which we do not include.

#### 5. Optimal moments

Used single moments

$$\omega^{(n,m)}(x) = (1-x)^n \sum_{k=0}^n (k+1)x^k \quad \text{with} \quad (n,m) = (1,0), (1,1), (1,2), (1,3), (1,4), (1,5), (2,0), (2,1), (2,2) \quad (4.1.7)$$

but omitted NPT corrections! He fitted the kinematic weight with free  $\alpha_s$  for  $\omega(x)^{(2,1)}$ . Later on he uses combined fits which is not in our interest. It is called optimal moments, because  $n$  stands for the pinching factor, which suppresses DV!

#### 6. Including information from the $s_0$ dependence

Pich fits  $A^{(2,0)}$ ,  $A^{(2,1)}$  and  $A^{(2,2)}$  separately for  $s_{\min} = 2 \text{ GeV}$ . The corresponding weights with fitted OPE dimensions are given by:

$$\omega^{(2,0)} = (1-x)^2 \quad c_4, c_6 \quad (4.1.8)$$

$$\omega^{(2,1)} = \omega_\tau \quad c_6, c_8 \quad (4.1.9)$$

$$\omega^{(2,2)} = (1-x)^2(1+2x+x^2) = (x^2-1)^2 \quad c_8, c_{10} \quad (4.1.10)$$

Thus we can compare our results from the kinematic weight with his results and furthermore add  $(1-x)^2$  to our fitting list?

Alpha is comparable, which just have a bigger error. For D6 and D8 we have to compare our definition of  $c_6, c_8$  with his.



## CHAPTER 5

# Derivation of the used inverse covariance matrix from the Aleph data

While performing a **Generalized least squares** (GLS) we estimate our regression coefficients  $\hat{\beta}$  as follows:

$$\hat{\beta} = \underset{\mathbf{b}}{\operatorname{argmin}} (\mathbf{y} - \mathbf{X}\mathbf{b})^T \mathbf{\Sigma}^{-1} (\mathbf{y} - \mathbf{X}\mathbf{b}), \quad (5.0.1)$$

with  $\mathbf{b}$  being an candidate estimate of  $\beta$ ,  $\mathbf{X}$  being the design matrix,  $\mathbf{y}$  being the response values and  $\mathbf{\Sigma}^{-1}$  being the **inverse covariance matrix**.

The Aleph data includes the **standard error** (SE), which are equal to the **standard deviation** as per definition. Furthermore Aleph provides the **correlation coefficients** of the errors. We will use these two quantities in combination with **Gaussian error propagation** to derive an approximation of the covariance matrix.

### 5.1 Propagation of experimental errors and correlation

Let  $\{f_k(x_1, x_2, \dots, x_n)\}$  be a set of  $m$  functions, which are linear combinations of  $n$  variables  $x_1, x_2, \dots, x_n$  with combination coefficients  $A_{k1}, A_{k2}, \dots, A_{kn}$ , where

$k \in \{1, 2, \dots, m\}$ . Let the covariance matrix of  $x_n$  be denoted by

$$\Sigma^x = \begin{pmatrix} \sigma_1^2 & \sigma_{12} & \sigma_{13} & \cdots \\ \sigma_{12} & \sigma_2^2 & \sigma_{23} & \cdots \\ \sigma_{13} & \sigma_{23} & \sigma_3^2 & \cdots \\ \vdots & \vdots & \vdots & \ddots \end{pmatrix}. \quad (5.1.1)$$

Then the covariance matrix of the functions  $\Sigma^f$  is given by

$$\Sigma_{ij}^f = \sum_k^n \sum_l^n A_{ik} \sum_{kl}^x A_{jl}, \quad \Sigma^f = A \Sigma^x A^T. \quad (5.1.2)$$

In our case we are dealing with non-linear functions, which we will linearized with the help of the **Taylor expansion**

$$f_k \approx f_k^0 + \sum_i^n \frac{\partial f_k}{\partial x_i} x_i, \quad f \approx f^0 + Jx. \quad (5.1.3)$$

Therefore, the propagation of error follows from the linear case, replacing the Jacobian matrix with the combination coefficients ( $J = A$ )

## CHAPTER 6

# Coefficients

### 6.1 $\beta$ function

There are several conventions for defining the  $\beta$  coefficients, depending on a minus sign and/or a factor of two (if one substitutes  $\mu \rightarrow \mu^2$ ) in the  $\beta$ -function [2.1.11](#). We follow the convention from Pascual and Tarrach (except for the minus sign) and have taken the values from [\[5\]](#)

$$\beta_1 = \frac{1}{6}(11N_c - 2N_f), \quad (6.1.1)$$

$$\beta_2 = \frac{1}{12}(17N_c^2 - 5N_cN_f - 3C_fN_f), \quad (6.1.2)$$

$$\beta_3 = \frac{1}{32} \left( \frac{2857}{54}N_c^3 - \frac{1415}{54}N_c^2N_f + \frac{79}{54}N_cN_f^2 - \frac{205}{18}N_cC_fN_f + \frac{11}{9}C_fN_f^2 + C_f^2N_f \right), \quad (6.1.3)$$

$$\beta_4 = \frac{140599}{2304} + \frac{445}{16}\zeta_3, \quad (6.1.4)$$

where we used  $N_f = 3$  and  $N_c = 3$  for  $\beta_4$ .

## 6.2 Anomalous mass dimension

$$\gamma_1 = \frac{3}{2}C_f, \quad (6.2.1)$$

$$\gamma_2 = \frac{C_f}{48}(97N_c + 9C_f - 10N_f), \quad (6.2.2)$$

$$\gamma_3 = \frac{C_f}{32} \left[ \frac{11413}{108}N_c^2 - \frac{129}{4}N_cC_f - \left( \frac{278}{27} + 24\zeta_3 \right) N_cN_f + \frac{129}{2}C_f^2 - (23 - 24\zeta_3)C_fN_f - \frac{35}{27}N_f^2 \right], \quad (6.2.3)$$

$$\gamma_4 = \frac{2977517}{20736} - \frac{9295}{216}\zeta_3 + \frac{135}{8}\zeta_4 - \frac{125}{6}\zeta_5, \quad (6.2.4)$$

where  $N_c$  is the number of colours,  $N_f$  the number of flavours and  $C_f = (N_c^2 - 1)/2N_c$ . We fixed furthermore fixed  $N_f = 3$  and  $N_c = 3$  for  $\gamma_4$ .

## 6.3 Adler function

# Bibliography

- [1] S. Aoki et al. “FLAG Review 2019”. In: (2019). arXiv: [1902.08191 \[hep-lat\]](#).
- [2] P. A. Baikov, K. G. Chetyrkin, and Johann H. Kuhn. “Order  $\alpha_s^4(s)$  QCD Corrections to Z and tau Decays”. In: *Phys. Rev. Lett.* 101 (2008), p. 012002. DOI: [10.1103/PhysRevLett.101.012002](#). arXiv: [0801.1821 \[hep-ph\]](#).
- [3] Martin Beneke, Diogo Boito, and Matthias Jamin. “Perturbative expansion of tau hadronic spectral function moments and  $\alpha_s$  extractions”. In: *JHEP* 01 (2013), p. 125. DOI: [10.1007/JHEP01\(2013\)125](#). arXiv: [1210.8038 \[hep-ph\]](#).
- [4] Martin Beneke and Matthias Jamin. “ $\alpha_s(s)$  and the tau hadronic width: fixed-order, contour-improved and higher-order perturbation theory”. In: *JHEP* 09 (2008), p. 044. DOI: [10.1088/1126-6708/2008/09/044](#). arXiv: [0806.3156 \[hep-ph\]](#).
- [5] Diogo Boito. “QCD phenomenology with  $\tau$  and charm decays”. PhD thesis. Universitat Autònoma de Barcelona, Sept. 2011.
- [6] Diogo Boito et al. “A new determination of  $\alpha_s$  from hadronic  $\tau$  decays”. In: *Phys. Rev. D* 84 (2011), p. 113006. DOI: [10.1103/PhysRevD.84.113006](#). arXiv: [1110.1127 \[hep-ph\]](#).
- [7] Diogo Boito et al. “Strong coupling from  $e^+e^- \rightarrow$  hadrons below charm”. In: *Phys. Rev. D* 98.7 (2018), p. 074030. DOI: [10.1103/PhysRevD.98.074030](#). arXiv: [1805.08176 \[hep-ph\]](#).
- [8] Diogo Boito et al. “Strong coupling from the revised ALEPH data for hadronic  $\tau$  decays”. In: *Phys. Rev. D* 91.3 (2015), p. 034003. DOI: [10.1103/PhysRevD.91.034003](#). arXiv: [1410.3528 \[hep-ph\]](#).

## BIBLIOGRAPHY

- [9] E. Braaten, Stephan Narison, and A. Pich. “QCD analysis of the tau hadronic width”. In: *Nucl. Phys.* B373 (1992), pp. 581–612. DOI: [10.1016/0550-3213\(92\)90267-F](https://doi.org/10.1016/0550-3213(92)90267-F).
- [10] David J. Broadhurst. “Chiral Symmetry Breaking and Perturbative QCD”. In: *Phys. Lett.* 101B (1981), pp. 423–426. DOI: [10.1016/0370-2693\(81\)90167-2](https://doi.org/10.1016/0370-2693(81)90167-2).
- [11] Irinel Caprini and Jan Fischer. “alpha(s) from tau decays: Contour-improved versus fixed-order summation in a new QCD perturbation expansion”. In: *Eur. Phys. J.* C64 (2009), pp. 35–45. DOI: [10.1140/epjc/s10052-009-1142-8](https://doi.org/10.1140/epjc/s10052-009-1142-8). arXiv: [0906.5211](https://arxiv.org/abs/0906.5211) [hep-ph].
- [12] Oscar Cata, Maarten Golterman, and Santi Peris. “Unraveling duality violations in hadronic tau decays”. In: *Phys. Rev.* D77 (2008), p. 093006. DOI: [10.1103/PhysRevD.77.093006](https://doi.org/10.1103/PhysRevD.77.093006). arXiv: [0803.0246](https://arxiv.org/abs/0803.0246) [hep-ph].
- [13] William Celmaster and Richard J. Gonsalves. “An Analytic Calculation of Higher Order Quantum Chromodynamic Corrections in  $e^+ e^-$  Annihilation”. In: *Phys. Rev. Lett.* 44 (1980), p. 560. DOI: [10.1103/PhysRevLett.44.560](https://doi.org/10.1103/PhysRevLett.44.560).
- [14] K. G. Chetyrkin, A. L. Kataev, and F. V. Tkachov. “Higher Order Corrections to Sigma-t ( $e^+ e^- \rightarrow$  Hadrons) in Quantum Chromodynamics”. In: *Phys. Lett.* 85B (1979), pp. 277–279. DOI: [10.1016/0370-2693\(79\)90596-3](https://doi.org/10.1016/0370-2693(79)90596-3).
- [15] M. Davier et al. “The Determination of alpha(s) from Tau Decays Revisited”. In: *Eur. Phys. J.* C56 (2008), pp. 305–322. DOI: [10.1140/epjc/s10052-008-0666-7](https://doi.org/10.1140/epjc/s10052-008-0666-7). arXiv: [0803.0979](https://arxiv.org/abs/0803.0979) [hep-ph].
- [16] Michel Davier, Andreas Hocker, and Zhiqing Zhang. “ALEPH Tau Spectral Functions and QCD”. In: *Nucl. Phys. Proc. Suppl.* 169 (2007). [22(2007)], pp. 22–35. DOI: [10.1016/j.nuclphysbps.2007.02.109](https://doi.org/10.1016/j.nuclphysbps.2007.02.109). arXiv: [hep-ph/0701170](https://arxiv.org/abs/hep-ph/0701170) [hep-ph].
- [17] Michel Davier, Andreas Höcker, and Zhiqing Zhang. “The physics of hadronic tau decays”. In: *Rev. Mod. Phys.* 78 (4 Oct. 2006), pp. 1043–1109. DOI: [10.1103/RevModPhys.78.1043](https://doi.org/10.1103/RevModPhys.78.1043). URL: <https://link.aps.org/doi/10.1103/RevModPhys.78.1043>.

## BIBLIOGRAPHY

- [18] Michel Davier et al. “Update of the ALEPH non-strange spectral functions from hadronic  $\tau$  decays”. In: *Eur. Phys. J. C* 74.3 (2014), p. 2803. DOI: [10.1140/epjc/s10052-014-2803-9](https://doi.org/10.1140/epjc/s10052-014-2803-9). arXiv: [1312.1501](https://arxiv.org/abs/1312.1501) [hep-ex].
- [19] Michael Dine and J. R. Sapirstein. “Higher Order QCD Corrections in  $e^+ e^-$  Annihilation”. In: *Phys. Rev. Lett.* 43 (1979), p. 668. DOI: [10.1103/PhysRevLett.43.668](https://doi.org/10.1103/PhysRevLett.43.668).
- [20] L. D. Faddeev and V. N. Popov. “Feynman Diagrams for the Yang-Mills Field”. In: *Phys. Lett. B* 25 (1967). [325(1967)], pp. 29–30. DOI: [10.1016/0370-2693\(67\)90067-6](https://doi.org/10.1016/0370-2693(67)90067-6).
- [21] H. Fritzsch, Murray Gell-Mann, and H. Leutwyler. “Advantages of the Color Octet Gluon Picture”. In: *Phys. Lett.* 47B (1973), pp. 365–368. DOI: [10.1016/0370-2693\(73\)90625-4](https://doi.org/10.1016/0370-2693(73)90625-4).
- [22] M. Gell-Mann. “Quarks”. In: *Acta Phys. Austriaca Suppl.* 9 (1972). [5(2015)], pp. 733–761. DOI: [10.1142/9789814618113\\_0002](https://doi.org/10.1142/9789814618113_0002), [10.1007/978-3-7091-4034-5\\_20](https://doi.org/10.1007/978-3-7091-4034-5_20).
- [23] S. G. Gorishnii, A. L. Kataev, and S. A. Larin. “The  $O(\alpha_s^3)$ -corrections to  $\sigma_{\text{tot}}(e^+e^- \rightarrow \text{hadrons})$  and  $\Gamma(\tau^- \rightarrow \nu_\tau + \text{hadrons})$  in QCD”. In: *Phys. Lett. B* 259 (1991), pp. 144–150. DOI: [10.1016/0370-2693\(91\)90149-K](https://doi.org/10.1016/0370-2693(91)90149-K).
- [24] D. J. Gross and Frank Wilczek. “Asymptotically Free Gauge Theories - I”. In: *Phys. Rev. D* 8 (1973), pp. 3633–3652. DOI: [10.1103/PhysRevD.8.3633](https://doi.org/10.1103/PhysRevD.8.3633).
- [25] Matthias Jamin. “Contour-improved versus fixed-order perturbation theory in hadronic tau decays”. In: *JHEP* 09 (2005), p. 058. DOI: [10.1088/1126-6708/2005/09/058](https://doi.org/10.1088/1126-6708/2005/09/058). arXiv: [hep-ph/0509001](https://arxiv.org/abs/hep-ph/0509001) [hep-ph].
- [26] Matthias Jamin. *QCD and Renormalisation Group Methods*. Lecture presented at Herbstschule für Hochenergiephysik Maria Laach. Sept. 2006.
- [27] Matthias Jamin and Manfred Munz. “Current correlators to all orders in the quark masses”. In: *Z. Phys. C* 60 (1993), pp. 569–578. DOI: [10.1007/BF01560056](https://doi.org/10.1007/BF01560056). arXiv: [hep-ph/9208201](https://arxiv.org/abs/hep-ph/9208201) [hep-ph].
- [28] Gunnar Kallen. “On the definition of the Renormalization Constants in Quantum Electrodynamics”. In: *Helv. Phys. Acta* 25 (417). [509(1952)]. DOI: [10.1007/978-3-319-00627-7\\_90](https://doi.org/10.1007/978-3-319-00627-7_90).

## BIBLIOGRAPHY

- [29] Alexander Keshavarzi, Daisuke Nomura, and Thomas Teubner. “Muon  $g - 2$  and  $\alpha(M_Z^2)$ : a new data-based analysis”. In: *Phys. Rev. D* 97.11 (2018), p. 114025. DOI: [10.1103/PhysRevD.97.114025](https://doi.org/10.1103/PhysRevD.97.114025). arXiv: [1802.02995](https://arxiv.org/abs/1802.02995) [hep-ph].
- [30] L. V. Lanin, V. P. Spiridonov, and K. G. Chetyrkin. “Contribution of Four Quark Condensates to Sum Rules for  $\rho$  and  $A_1$  Mesons. (In Russian)”. In: *Yad. Fiz.* 44 (1986), pp. 1372–1374.
- [31] F. Le Diberder and A. Pich. “Testing QCD with tau decays”. In: *Phys. Lett. B* 289 (1992), pp. 165–175. DOI: [10.1016/0370-2693\(92\)91380-R](https://doi.org/10.1016/0370-2693(92)91380-R).
- [32] H. Lehmann. “On the Properties of propagation functions and renormalization constants of quantized fields”. In: *Nuovo Cim.* 11 (1954), pp. 342–357. DOI: [10.1007/BF02783624](https://doi.org/10.1007/BF02783624).
- [33] R. Tarrach P. Pascual. *QCD: Renormalization for the Practitioner*. Springer-Verlag, 1984.
- [34] Michael E. Peskin and Daniel V. Schroeder. *An Introduction to quantum field theory*. Reading, USA: Addison-Wesley, 1995. URL: <http://www.slac.stanford.edu/~mpeskin/QFT.html>.
- [35] Antonio Pich. “Precision Tau Physics”. In: *Prog. Part. Nucl. Phys.* 75 (2014), pp. 41–85. DOI: [10.1016/j.ppnp.2013.11.002](https://doi.org/10.1016/j.ppnp.2013.11.002). arXiv: [1310.7922](https://arxiv.org/abs/1310.7922) [hep-ph].
- [36] Antonio Pich and Joaquim Prades. “Strange quark mass determination from Cabibbo suppressed tau decays”. In: *JHEP* 10 (1999), p. 004. DOI: [10.1088/1126-6708/1999/10/004](https://doi.org/10.1088/1126-6708/1999/10/004). arXiv: [hep-ph/9909244](https://arxiv.org/abs/hep-ph/9909244) [hep-ph].
- [37] Antonio Pich and Antonio Rodríguez-Sánchez. “Determination of the QCD coupling from ALEPH  $\tau$  decay data”. In: *Phys. Rev. D* 94 (3 Aug. 2016), p. 034027. DOI: [10.1103/PhysRevD.94.034027](https://doi.org/10.1103/PhysRevD.94.034027). URL: <https://link.aps.org/doi/10.1103/PhysRevD.94.034027>.
- [38] H. David Politzer. “Reliable Perturbative Results for Strong Interactions?”. In: *Phys. Rev. Lett.* 30 (1973). [274(1973)], pp. 1346–1349. DOI: [10.1103/PhysRevLett.30.1346](https://doi.org/10.1103/PhysRevLett.30.1346).



## BIBLIOGRAPHY

- [39] Eduardo de Rafael. “An Introduction to sum rules in QCD: Course”. In: *Probing the standard model of particle interactions. Proceedings, Summer School in Theoretical Physics, NATO Advanced Study Institute, 68th session, Les Houches, France, July 28-September 5, 1997. Pt. 1, 2.* 1997, pp. 1171–1218. arXiv: [hep-ph/9802448](#) [[hep-ph](#)].
- [40] S. Schael et al. “Branching ratios and spectral functions of tau decays: Final ALEPH measurements and physics implications”. In: *Phys. Rept.* 421 (2005), pp. 191–284. DOI: [10.1016/j.physrep.2005.06.007](#). arXiv: [hep-ex/0506072](#) [[hep-ex](#)].
- [41] Felix Schwab. “Strange Quark Mass Determination From Sum Rules For Hadronic  $\tau$ -Decays”. German. MA thesis. somewhere, 2002.
- [42] Mikhail A. Shifman, A. I. Vainshtein, and Valentin I. Zakharov. “QCD and Resonance Physics: Applications”. In: *Nucl. Phys.* B147 (1979), pp. 448–518. DOI: [10.1016/0550-3213\(79\)90023-3](#).
- [43] Mikhail A. Shifman, A. I. Vainshtein, and Valentin I. Zakharov. “QCD and Resonance Physics. Theoretical Foundations”. In: *Nucl. Phys.* B147 (1979), pp. 385–447. DOI: [10.1016/0550-3213\(79\)90022-1](#).
- [44] Levan R. Surguladze and Mark A. Samuel. “Total hadronic cross-section in  $e^+e^-$  annihilation at the four loop level of perturbative QCD”. In: *Phys. Rev. Lett.* 66 (1991). [Erratum: *Phys. Rev. Lett.* 66, 2416 (1991)], pp. 560–563.
- [45] M. Tanabashi et al. “Review of Particle Physics”. In: *Phys. Rev.* D98.3 (2018), p. 030001. DOI: [10.1103/PhysRevD.98.030001](#).
- [46] Yung-Su Tsai. “Decay Correlations of Heavy Leptons in  $e^+ + e^- \rightarrow l^+ + l^-$ ”. In: *Phys. Rev. D* 4 (9 Nov. 1971), pp. 2821–2837. DOI: [10.1103/PhysRevD.4.2821](#). URL: <https://link.aps.org/doi/10.1103/PhysRevD.4.2821>.
- [47] Steven Weinberg. “Nonabelian Gauge Theories of the Strong Interactions”. In: *Phys. Rev. Lett.* 31 (1973), pp. 494–497. DOI: [10.1103/PhysRevLett.31.494](#).
- [48] Steven Weinberg. “Phenomenological Lagrangians”. In: *Physica* A96.1-2 (1979), pp. 327–340. DOI: [10.1016/0378-4371\(79\)90223-1](#).

## BIBLIOGRAPHY

- [49] Kenneth G. Wilson. “Confinement of quarks”. In: *Phys. Rev. D* 10 (8 Oct. 1974), pp. 2445–2459. DOI: [10.1103/PhysRevD.10.2445](https://doi.org/10.1103/PhysRevD.10.2445). URL: <https://link.aps.org/doi/10.1103/PhysRevD.10.2445>.
- [50] Kenneth G. Wilson. “Nonlagrangian models of current algebra”. In: *Phys. Rev.* 179 (1969), pp. 1499–1512. DOI: [10.1103/PhysRev.179.1499](https://doi.org/10.1103/PhysRev.179.1499).

# List of Abbreviations

NPT	Non-Perturbative Theory, page 7
NP	Non-Perturbative, page 7
OPE	Operator Product Expansion, page 18
PT	Perturbative Theory, page 7
QCD	Quantum Chromodynamics, page 4
QFT	Quantum Field Theory, page 3
RGE	Renormalisation Group Equation, page 9
SM	Standard Model, page 3
CHPT	Chiral Perturbation Theory, page 7
LQCD	Lattice Quantum Chromodynamics, page 8
QCDSR	Quantum Chromodynamics Sum Rules, page 8